AGU PUBLICATIONS

Paleoceanography

RESEARCH ARTICLE
10.1002/2015PA002794

Holocene variability in the intensity of wind-gap upwelling in the tropical eastern Pacific

Lauren T. Toth[1,2], Richard B. Aronson[1], Hai Cheng[3,4], and R. Lawrence Edwards[4]

[1]Department of Biological Sciences, Florida Institute of Technology, Melbourne, Florida, USA, [2]Coastal and Marine Science Center, U.S. Geological Survey, Saint Petersburg, Florida, USA, [3]Institute of Global Environmental Change, Xi'an Jiaotong University, Xi'an, China, [4]Department of Earth Sciences, University of Minnesota, Minneapolis, Minnesota, USA

Key Points:
- The wind-gap upwelling system in Pacific Panamá was present by ~6750 cal B.P.
- Modern upwelling in the Gulf of Panamá was weak relative to the middle Holocene
- ENSO was the primary driver of upwelling in Pacific Panamá during the Holocene

Supporting Information:
- Tables S1 and S2

Correspondence to:
L. T. Toth,
ltoth@usgs.gov

Citation:
Toth, L. T., R. B. Aronson, H. Cheng, and R. L. Edwards (2015), Holocene variability in the intensity of wind-gap upwelling in the tropical eastern Pacific, *Paleoceanography*, *30*, 1113–1131, doi:10.1002/2015PA002794.

Received 18 FEB 2015
Accepted 21 JUL 2015
Accepted article online 25 JUL 2015
Published online 24 AUG 2015

Abstract Wind-driven upwelling in Pacific Panamá is a significant source of oceanographic variability in the tropical eastern Pacific. This upwelling system provides a critical teleconnection between the Atlantic and tropical Pacific that may impact climate variability on a global scale. Despite its importance to oceanographic circulation, ecology, and climate, little is known about the long-term stability of the Panamanian upwelling system or its interaction with climatic forcing on millennial time scales. Using a combination of radiocarbon and U-series dating of fossil corals collected in cores from five sites across Pacific Panamá, we reconstructed the local radiocarbon reservoir correction, ΔR, from ~6750 cal B.P. to present. Because the ΔR of shallow-water environments is elevated by upwelling, our data set represents a millennial-scale record of spatial and temporal variability of the Panamanian upwelling system. The general oceanographic gradient from relatively strong upwelling in the Gulf of Panamá to weak-to-absent upwelling in the Gulf of Chiriquí was present throughout our record; however, the intensity of upwelling in the Gulf of Panamá varied significantly through time. Our reconstructions suggest that upwelling in the Gulf of Panamá is weak at present; however, the middle Holocene was characterized by periods of enhanced upwelling, with the most intense upwelling occurring just after of a regional shutdown in the development of reefs at ~4100 cal B.P. Comparisons with regional climate proxies suggest that, whereas the Intertropical Convergence Zone is the primary control on modern upwelling in Pacific Panamá, the El Niño–Southern Oscillation drove the millennial-scale variability of upwelling during the Holocene.

1. Introduction

The regional pattern of oceanographic and atmospheric circulation in the tropical eastern Pacific (TEP) is an important driver of global-scale variability in climate, oceanic productivity, and the distribution of marine organisms [*Pennington et al.*, 2006; *Poveda et al.*, 2006]. On the largest spatial scales, circulation in the TEP is dominated by the Peruvian (PC), Californian (CC), and equatorial upwelling systems; east-to-west surface transport by the North and South Equatorial Currents (NEC and SEC); and west-to-east transport by the North Equatorial Countercurrent (NECC) and the subsurface Equatorial Undercurrent (EUC) (Figure 1a) [*Wyrtki*, 1965; *Kessler*, 2006; *Leduc et al.*, 2009b]. Overprinting these major current patterns are a number of significant, mesoscale oceanographic heterogeneities throughout the region, most notably a series of localized upwelling systems along the Central American coast (Figure 1a) [*Kessler*, 2006; *Alexander et al.*, 2012]. These systems represent a critical teleconnection between the Atlantic and Pacific that may contribute to climatic variability on a global scale [*Timmermann et al.*, 2007; *Xie et al.*, 2008].

Seasonal, wind-driven upwelling occurs in three locations where topographic lows in the Central American Cordillera allow strong easterly wind jets to reach the eastern Pacific: the Gulf of Tehuantepec in Mexico, the Gulf of Papagayo in Costa Rica, and the Gulf of Panamá (Figure 1a). During the boreal winter, persistent winds of ~6 m s^{-1} and wind bursts up to 30 m s^{-1} occur in these "wind-gap" systems. Surface mixing and thermocline shoaling depress water temperatures [*Pennington et al.*, 2006; *Alexander et al.*, 2012], elevate nutrients and salinity [*Kessler*, 2006; *Pennington et al.*, 2006; *D'Croz and O'Dea*, 2007], and lower the pH [*Manzello et al.*, 2008] and dissolved oxygen [*Kessler*, 2006] of the surface waters from coastal areas to hundreds of kilometers offshore [*Alexander et al.*, 2012]. These mesoscale oceanographic features represent a significant source of interannual variability in the coastal TEP [*Xie et al.*, 2008] and are an important control on the oceanic productivity and biogeography of the region's marine ecosystems.

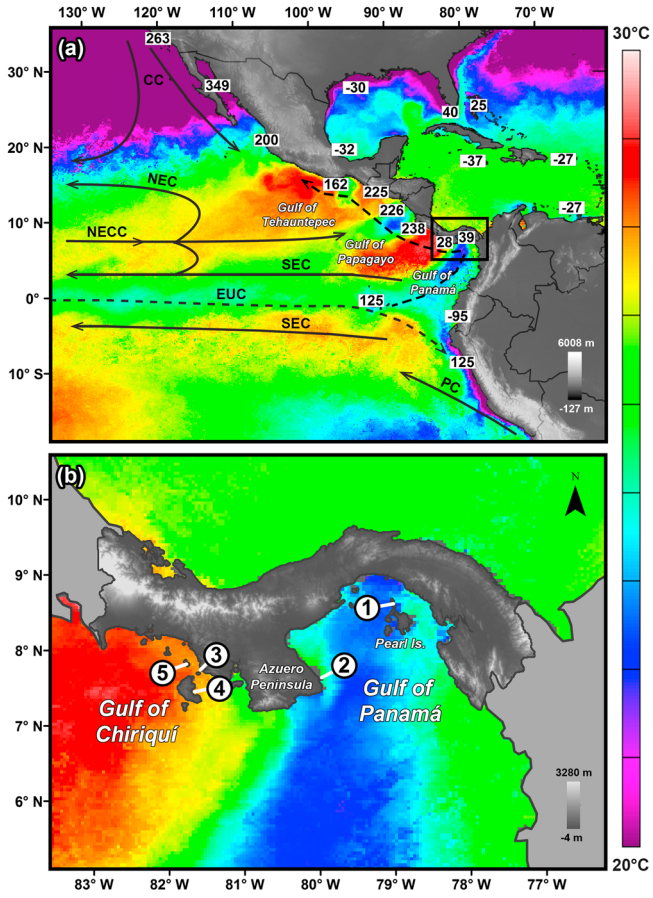

Figure 1. Illustration of the regional oceanography of the TEP. Coloration shows sea surface temperature (SST) at the peak of the 2009 upwelling season in Panamá, 4–17 March. (a) Existing records of modern ΔR values for the TEP from the 14CHRONO Marine Reservoir Database (http://calib.qub.ac.uk/marine/, and references therein) and Caribbean in relation to the major surface (solid black lines) and sub-surface (dashed lines) current systems of the region and the location of the three upwelling centers in the tropical eastern Pacific: the Gulf of Tehauntepec, the Gulf of Papagayo, and the Gulf of Panamá. Regional topography (250 m resolution) is displayed in gray scale. (b) The area shown in black outline in Figure 1a is expanded. Mesoscale oceanography of Pacific Panamá is shown in relation to the topography of the Panamanian Isthmus (90 m resolution) and the location of the five study sites: (1) Contadora, (2) Iguana, (3) Canales de Tierra, (4) Coiba, and (5) Uva. The SST imagery was created from Moderate Resolution Imaging Spectroradiometer/Aqua Satellite SST data using NASA's Physical Oceanography Distributed Active Archive software (http://podaac.jpl.nasa.gov/). The digital elevation data were obtained from the Consultative Group on International Agricultural Research Consortium for Spatial Information (http://srtm.csi.cgiar.org/).

Although they account for a small geographic area, the wind-gap systems are responsible for more than 2.5% of the primary production in the TEP and nearly 1% of the total primary productivity in the Pacific Ocean [*Pennington et al.*, 2006]. Upwelling is also an important control on the growth and distribution of coral-reef habitats in the TEP [*Toth*, 2013]. In the Gulf of Panamá, for example, development of coral reefs is restricted to small embayments that are sheltered from oceanographic influence [*Glynn and Stewart*, 1973]. Rates of coral growth are significantly slower than in the nearby Gulf of Chiriquí, where there is no upwelling (Figure 1b) [*Glynn*, 1977]. Reef frameworks are also considerably thicker in the Gulf of Chiriquí than in the Gulf of Panamá, presumably because of the long-term impact of upwelling on reef growth [*Glynn and Macintyre*, 1977].

Reefs in Pacific Panamá and Costa Rica experienced a 2500 year hiatus in reef growth, from ~4100 to 1600 cal B.P. (calibrated calendar years before 1950 [*Toth et al.*, 2012]). The hiatus was related to an increase in the strength and variability of the El Niño–Southern Oscillation (ENSO) and changes in the position of the Intertropical Convergence Zone (ITCZ) [*Toth et al.*, 2012, 2015]. Because of the negative impact of upwelling, the hiatus lasted longer in the Gulf of Panamá than in the Gulf of Chiriquí [*Toth et al.*, 2012]. In a similar fashion, suppression of reef development in the Gulf of Papagayo in recent centuries has been linked to a period of enhanced upwelling during the Little Ice Age [*Glynn et al.*, 1983].

The interaction between climate and upwelling in driving millennial-scale coral-reef dynamics suggests that the intensity of upwelling in the wind-gap systems may have varied significantly during the Holocene. The definition of the early, middle, and late Holocene periods vary markedly in the literature [*Karamperidou et al.*, 2015]; however, in the discussions that follow, we always refer to the period until ~7000 years ago as the early Holocene, ~7000–4000 years ago as the middle Holocene, and ~4000 years ago to present as the late Holocene, unless otherwise specified.

Although the regional oceanography produced by modern upwelling in the wind-gap systems has been well characterized in recent decades (reviewed in *Kessler* [2006]), little is known about how these systems behaved in the past. In the present study, we use coral-based records of radiocarbon variability to characterize the spatial and temporal variability of the Panamanian wind-gap upwelling system during the Holocene. We

compare our reconstruction with records of regional climate to determine the primary drivers of upwelling variability in the past and to predict the likely trends in wind-gap upwelling in the future.

2. Climatic Forcing in the TEP

The general atmospheric and oceanographic phenomena responsible for creating the wind-gap upwelling centers have been in place for at least the last 7000 years [*Martínez et al.*, 2006; *Toth et al.*, 2012]. In fact, the Panamanian upwelling system may have been established as early as the mid-Pleistocene [*O'Dea et al.*, 2012]. It is likely, however, that the intensity of upwelling at these locations has been modulated by large-scale climatic oscillations through the Holocene. At present, the ITCZ and ENSO are the primary drivers of climatic, atmospheric, and oceanographic variability in the TEP [*Martínez et al.*, 2006; *Pennington et al.*, 2006; *Poveda et al.*, 2006]. The millennial-scale dynamics of these two phenomena and their interactions with larger-scale climatic forcing were therefore the most likely control on variability in the wind-gap systems during the Holocene.

In the Gulfs of Papagayo and Panamá, upwelling is driven by seasonal intensification of the northeast trade winds, a process that is initiated by the annual southerly migration of the ITCZ during the boreal winter [*Pennington et al.*, 2006; *Poveda et al.*, 2006; *Alexander et al.*, 2012]. (Upwelling in the Gulf of Tehuantepec is primarily driven by wind bursts from midlatitude storms [*Alexander et al.*, 2012] and is therefore not strongly related to the ITCZ.) Over an annual cycle, the modern ITCZ is found between ~10°N and 1°S latitude in the TEP, following the peak in insolation [*Martínez et al.*, 2006; *Poveda et al.*, 2006; *Schneider et al.*, 2014]; however, its mean position has varied significantly on centennial to millennial time scales as a result of climatic forcing [*Peterson et al.*, 2000; *Haug et al.*, 2001; *Peterson and Haug*, 2006; *Leduc et al.*, 2009a; *Sachs et al.*, 2009; *Schneider et al.*, 2014].

In general, the ITCZ has occupied a more northerly position in the tropical Pacific during warm periods (interstadials) and has moved to the south during cool periods (stadials) [*Peterson et al.*, 2000; *Peterson and Haug*, 2006; *Sachs et al.*, 2009; *Schneider et al.*, 2014]. Records from the Cariaco Basin in Venezuela suggest that the ITCZ occupied its most northerly position in the TEP during the early through middle Holocene (~10,000–4500 years ago) and has since gradually been moving to the south [*Haug et al.*, 2001; *Peterson and Haug*, 2006; *Schneider et al.*, 2014]. The millennial-scale changes in the position of the ITCZ were likely driven by latitudinal shifts in seasonality of insolation [*Schneider et al.*, 2014]. Whereas boreal summer insolation was higher in the Northern Hemisphere during the early and middle Holocene, summer insolation was stronger in the Southern Hemisphere by the late Holocene [*Haug et al.*, 2001; *Schneider et al.*, 2014]. It is generally assumed that a more southerly position of the ITCZ after the middle Holocene would have strengthened the northeast trade winds and, therefore, that the strength of upwelling and the seasonality in Costa Rica and Panamá should have generally increased toward the present [*Haug et al.*, 2001; *Martínez et al.*, 2006].

The strength of wind-gap upwelling, and the position of the ITCZ, have also been linked to remote climatic forcing in the northern Atlantic [*Timmermann et al.*, 2007; *Xie et al.*, 2008; *Arellano-Torres et al.*, 2013; *Schneider et al.*, 2014]. Specifically, modeling suggests that cooling in the North Atlantic and the associated weakening of the Atlantic meridional overturning circulation lead to an increase in atmospheric pressure across the Caribbean. The enhanced meridional pressure gradient across the Atlantic strengthens the northeast trade winds, which drives the ITCZ to the south [*Timmermann et al.*, 2007; *Xie et al.*, 2008; *Leduc et al.*, 2009a; *Schneider et al.*, 2014]. Thus, cooling (or warming) of the North Atlantic should be associated with increased (or decreased) wind-gap upwelling. Both modeling experiments and proxy data suggest that the northern Atlantic gradually cooled after the middle Holocene [*Marcott et al.*, 2013; *Liu et al.*, 2014a], which is in agreement with the overall southerly migration of the ITCZ to present [*Haug et al.*, 2001; *Peterson and Haug*, 2006; *Schneider et al.*, 2014]. An increase in wind-gap upwelling after the middle Holocene would be expected from northern Atlantic cooling and the southerly migration of the ITCZ [*Martínez et al.*, 2006; *Timmermann et al.*, 2007; *Xie et al.*, 2008].

ENSO variability results in marked changes in both wind-driven upwelling and the basin-wide tilt of the thermocline in the Pacific [*Pennington et al.*, 2006]. Trade winds are generally weakened or reversed during an El Niño event due to the migration of the center of atmospheric convection to the middle of the Pacific Basin [*Philander*, 1990]; however, regional oceanic warming can cause local wind speeds in the coastal upwelling centers in the Gulf of Panamá, Papagayo, and Tehauntepec to increase during El Niño events [*Alexander et al.*, 2012]. Despite the stronger localized winds during El Niño years, true upwelling is generally suppressed during El Niño events, because El Niño also results in a deepening of the thermocline [*Philander*, 1990; *Pennington et al.*, 2006]. Although the impact of ENSO on upwelling is complex, the net effect is a

reduction in wind-gap upwelling during El Niño and enhanced upwelling during La Niña [*Philander*, 1990; *Pennington et al*., 2006; *Poveda et al*., 2006].

There are two dominant spatial modes of ENSO based on the location of maximum sea surface temperature anomalies: the central Pacific and the eastern Pacific ENSOs [*Carré et al*., 2014; *Karamperidou et al*., 2015]. Recent studies have demonstrated that inconsistencies in reconstructions of Holocene ENSO variability from various locations throughout the Pacific may be the result of changes in the spatial manifestation of ENSO in the past [*Carré et al*., 2014; *Karamperidou et al*., 2015]. For example, whereas proxy records from the TEP suggest that there was a significant decline in ENSO variability during the middle Holocene, records from the central Pacific show no significant change during this period [*Koutavas et al*., 2002, 2006; *Koutavas and Joanides*, 2012; *Cobb et al*., 2013; *Carré et al*., 2014; *Karamperidou et al*., 2015]. Because of the spatial asymmetry of ENSO dynamics, we generally focus our discussion of Holocene ENSO variability on records that are specific to the TEP, but we also draw on records from the broader tropical Pacific where appropriate.

Across millennial time scales, the mean state of the tropical Pacific is often described in terms of "El Niño-like" or "La Niña-like" climates [e.g., *Koutavas et al*., 2002; *Stott et al*., 2002; *Conroy et al*., 2008; *Toth et al*., 2015]. ENSO-like climates are characterized by trends in long-term climatic conditions that are analogous to changes that occur over an ENSO cycle [*Koutavas et al*., 2002; *Stott et al*., 2002]. Thus, in the TEP, warm periods with low oceanographic productivity are more El Niño-like, whereas cool periods with high oceanographic productivity are more La Niña-like [*Stott et al*., 2002; *Toth et al*., 2015]. Using proxy-based records of climate change in the past, it is often difficult to discern whether periods of El Niño-like or La Niña-like climates were directly driven by shifts in ENSO variability or were simply the result of regional changes in the mean climate state or in seasonality [*Stott et al*., 2002]. When possible, we examine changes in upwelling in relation to ENSO variability per se, but we also discuss shifts in mean climate in the TEP in terms of ENSO-like conditions.

In contrast with the gradual changes in northern Atlantic climate and the ITCZ, ENSO was highly variable during the Holocene [*Cobb et al*., 2013; *Rein et al*., 2005; *Koutavas et al*., 2006; *Rein*, 2007; *Conroy et al*., 2008; *Koutavas and Joanides*, 2012; *Liu et al*., 2014b]. Variability in both ENSO and the ITCZ increased after ~4500–4000 cal B.P. [*Corrège et al*., 2000; *Haug et al*., 2001; *Rein et al*., 2005; *Peterson and Haug*, 2006; *Rein*, 2007; *Conroy et al*., 2008; *Koutavas and Joanides*, 2012; *Carré et al*., 2014; *Liu et al*., 2014b] and remained high during the next 2000 years [*Haug et al*., 2001; *Rein et al*., 2005; *Peterson and Haug*, 2006; *Rein*, 2007; *Conroy et al*., 2008; *Carré et al*., 2014]. The synchronization of these two important controls on the regional oceanography of the TEP [*Haug et al*., 2001; *Peterson and Haug*, 2006] suggests that variability in the wind-gap upwelling centers may have been particularly high at that time.

By the late Holocene, however, the oceanographic forcing by ENSO and the ITCZ would have driven divergent responses in wind-gap upwelling. In the TEP, the middle Holocene was characterized by a cool, La Niña-like climate and low ENSO variability [*Koutavas et al*., 2002, 2006; *Koutavas and Joanides*, 2012; *Cabarcos et al*., 2014; *Karamperidou et al*., 2015], whereas ENSO variability has increased in recent millennia [*Koutavas et al*., 2006; *Makou et al*., 2010; *Koutavas and Joanides*, 2012; *Carré et al*., 2014; *Liu et al*., 2014b]. A number of records from the TEP suggest that the frequency of El Niño was particularly high during the last several millennia [*Sandweiss et al*., 2001; *Moy et al*., 2002; *Riedinger et al*., 2002; *Conroy et al*., 2008, 2009]. With the exception of the Little Ice Age, which was likely characterized by a La Niña-like climate in the TEP [*Conroy et al*., 2009; *Toth et al*., 2015], the late Holocene was dominated by an El Niño-like state [*Koutavas and Joanides*, 2012; *Cabarcos et al*., 2014]. The general shift in the mode of ENSO, and the increase in the frequency of El Niño events, would have acted in opposition to the forcing by northern Atlantic cooling and the resulting southerly movement of the ITCZ in the late Holocene and would have favored a decline in regional productivity from the middle to the late Holocene [*Pennington et al*., 2006]. Such uncertainties highlight the need for comprehensive, high-resolution records of upwelling from the wind-gap systems to discern both the relative importance of large-scale climatic drivers and the impact that changes in upwelling may have had on ecosystems during the Holocene.

3. Radiocarbon-Based Reconstructions of Upwelling

Radiocarbon ages of marine organisms such as corals are strongly influenced by the radiocarbon age of the local water mass [*Bard et al*., 1993; *Reimer and Reimer*, 2001; *Reimer et al*., 2009]. On a global scale, the apparent radiocarbon age of the oceanic mixed layer—the global marine reservoir age, *R*—is determined by both variability in atmospheric ^{14}C production and long-term mixing with oceanic deep water, which is depleted

in radiocarbon relative to the atmosphere [*Reimer and Reimer*, 2001; *Druffel et al*., 2008; *Zaunbrecher et al*., 2010]. Global reservoir ages ranged between ~270 and 470 years during the Holocene [*Reimer and Reimer*, 2001; *Reimer et al*., 2009], but the true offset between marine and atmospheric radiocarbon ratios at any given location is also impacted by mesoscale differences in vertical water-column mixing [*Druffel et al*., 2008; *Zaunbrecher et al*., 2010].

The local reservoir correction, ΔR, is a measure of the divergence between the global and local reservoir ages and therefore provides a powerful proxy for changes in water-column mixing in the past. Whereas ΔR is negligible in places with strong water-column stratification or downwelling [*Druffel et al*., 2008; *Zaunbrecher et al*., 2010], it is high in regions influenced by upwelling [*Ingram*, 1998; *Fontugne et al*., 2004; *Soares and Dias*, 2006; *Zaunbrecher et al*., 2010]. The higher modern values of ΔR throughout the TEP region relative to the Caribbean and, on a smaller scale, in the Gulf of Panamá relative to the Gulf of Chiriquí (Figure 1 and Table 1; from the coral-based records of this study and *Druffel* [1987]), demonstrate the sensitivity of this proxy to upwelling gradients across multiple spatial scales.

We reconstructed spatial and temporal variability in upwelling during discrete points in time from ~6750 cal B.P. to present by measuring ΔR in subfossil, shallow-water corals across Pacific Panamá to test the following hypotheses: (1) the modern upwelling gradient in Pacific Panamá was present throughout the Holocene, (2) upwelling intensity varied significantly during the Holocene and is lowest at present because of the increased frequency of El Niño in recent millennia [*Sandweiss et al*., 2001; *Moy et al*., 2002; *Riedinger et al*., 2002; *Conroy et al*., 2008, 2009], and (3) upwelling intensity increased leading up to the hiatus in coral-reef development ~4100–1600 cal B.P. [*Toth et al*., 2012, 2015]. We also compared temporal trends in ΔR with regional climate records to evaluate the influence of large-scale climatic oscillations on the intensity of wind-gap upwelling in the past.

4. Oceanographic Setting

Seasonal upwelling is the most important source of intra-annual variability in the marine environments of Pacific Panamá. Upwelling coincides with Panamá's dry season—December through mid-April—when the meridional migration of the ITCZ allows for the regional intensification of the northeast trade winds [*Pennington et al*., 2006; *Poveda et al*., 2006]. Because of the topographic differential along the Panamanian Isthmus, there is a pronounced gradient in upwelling strength along Panamá's Pacific coast (Figure 1b). The Pearl Islands archipelago is located adjacent to a topographic low in the Central American Cordillera, which allows strong wind jets to pass over this region. Ekman pumping driven by positive wind-stress curl produces strong upwelling across the archipelago [*Kessler*, 2006; *Pennington et al*., 2006; *Alexander et al*., 2012]. Intermediate upwelling occurs in the western Gulf of Panamá along the eastern side of the Azuero Peninsula. Upwelling is absent in the Gulf of Chiriquí, where the elevated topography of the isthmus creates negative wind-stress curl, and downwelling is the dominant oceanographic process [*Pennington et al*., 2006; *Alexander et al*., 2012].

5. Methods

5.1. Collection and Dating of the Fossil Coral Samples

Push cores were extracted from the unconsolidated reef frameworks at five sites across the contemporary gradient of upwelling along Panamá's Pacific coast (Figure 1b). We collected cores from two sites within the Gulf of Panamá upwelling center: Contadora and Iguana Islands. Contadora, in the Pearl Islands archipelago, is subject to the most intense and consistent seasonal upwelling. Upwelling is moderate and temporally variable at Iguana Island off the southeastern tip of the Azuero Peninsula. We also collected cores from three sites in the Gulf of Chiriquí—Coiba, Canales de Tierra, and Uva Islands—where there is putatively no upwelling (Figure 1b).

The cores were extruded either in the field or in the laboratory, and the recovered material was divided into 5 cm segments. Each 5 cm segment was sieved, and core constituents >2 mm in longest dimension were cleaned using high-pressure water and dried overnight at 105°C. Sediments >2 mm, almost all of which were fragments of *Pocillopora* spp. corals, were sorted by species and techonomic condition. For detailed coring and core processing methodologies, see *Toth et al.* [2012].

We dated 42 corals in excellent taphomonic condition from cores collected at Contadora ($N = 12$) and Iguana Islands ($N = 10$) in the Gulf of Panamá and Coiba ($N = 7$), Canales de Tierra ($N = 8$) and Uva Islands ($N = 5$) in the Gulf of Chiriquí (see Figure 1b for geographic locations). These samples represent a data set extended from

Table 1. Calibrated U/Th Ages and Uncalibrated, "Conventional" ^{14}C Ages and the Corresponding R and ΔR Values of Coral Samples From Contadora, Iguana, Coiba, Canales de Tierra, and Uva Islands

Gulf	Site	U/Th Age[a]	^{14}C Age	R[b]	ΔR[b]
Panamá	*Contadora*	212 ± 7[c]	600 ± 49	439 ± 51	60 ± 67
		978 ± 12	1520 ± 78	424 ± 82	71 ± 92
		1450 ± 8	2030 ± 78	441 ± 82	129 ± 94
		1630 ± 22[e]	2130 ± 78	379 ± 82	61 ± 94
		3793 ± 22	4380 ± 25	773 ± 57	560 ± 72*
		4289 ± 13	4600 ± 39	733 ± 46	400 ± 63*[d]
		4322 ± 19	4590 ± 78	693 ± 82	377 ± 94*
		5096 ± 27	5080 ± 78	555 ± 82	256 ± 94*
		5271 ± 20	5060 ± 59	569 ± 63	145 ± 77
		6761 ± 35	6570 ± 78	617 ± 83	263 ± 94*
	Iguana	**52 ± 14**	**495 ± 49**	**421 ± 51**[f]	**39 ± 67**[f]
		1157 ± 11	1870 ± 78	670 ± 81	291 ± 92*
		1243 ± 25	1830 ± 59	556 ± 64	162 ± 78
		1323 ± 16	1820 ± 78	382 ± 82	30 ± 94
		4162 ± 101[e]	4480 ± 78	664 ± 82	361 ± 94*
		4426 ± 32	4430 ± 59	449 ± 64	114 ± 78
		4440 ± 12	4580 ± 78	578 ± 82	249 ± 92*
		4731 ± 22	4580 ± 39	396 ± 46	71 ± 63
		5427 ± 27	5360 ± 78	690 ± 81	315 ± 92*
Chiriquí	*Coiba*	367 ± 11	815 ± 39	482 ± 42	96 ± 60
		1885 ± 14	2280 ± 88	339 ± 92	−2 ± 102
		4310 ± 24	4400 ± 59	504 ± 64	189 ± 78*
		4384 ± 21	4310 ± 69	420 ± 72	57 ± 84
		4938 ± 24	4730 ± 49	358 ± 54	20 ± 69
		4971 ± 18	4900 ± 39	499 ± 47	156 ± 64*
		6566 ± 24	6280 ± 49	503 ± 57	145 ± 72*
	Canales de Tierra	268 ± 13	725 ± 49	568 ± 51	110 ± 67
		1424 ± 10	1940 ± 59	355 ± 63	39 ± 78
		1506 ± 39	1980 ± 59	417 ± 64	39 ± 78
		3980 ± 19	4130 ± 59	468 ± 64	139 ± 78*
		4009 ± 21	4020 ± 59	310 ± 64	10 ± 78
		4264 ± 17	4300 ± 49	434 ± 55	117 ± 71
		4425 ± 16	4330 ± 59	350 ± 64	15 ± 78
		4429 ± 17	4380 ± 59	395 ± 64	61 ± 78
	Uva	**modern**			**28 ± 31**[f]
		122 ± 11	600 ± 49	502 ± 51	102 ± 67
		3147 ± 31	3220 ± 59	258 ± 66	−81 ± 79
		3163 ± 24	3470 ± 59	492 ± 64	152 ± 78*
		4335 ± 19	4320 ± 59	442 ± 64	102 ± 78
		4612 ± 33	4640 ± 59	523 ± 63	191 ± 77*

[a] U/Th ages are given in cal B.P. (calibrated calendar years before 1950).
[b] R and ΔR are reported in years. See equations (1) and (2) for the explanation of the calculations.
[c] All errors are reported as 95% confidence intervals (CI; 1.96*σ). See equation (3) for the calculation of σ.
[d] ΔR values that are significantly different from modern (i.e., their 95% CI do not overlap with the modern value for that gulf) are indicated with an asterisk.
[e] The two samples from *Psammocora* spp. corals that were dated. All other samples were *Pocillopora* spp.
[f] Modern values for ΔR from the Gulf of Panamá (from the present study) and the Gulf of Chiriquí [*Druffel*, 1987] are indicated in bold.

that presented in *Toth et al.* [2012], in which the ΔR values reported from Canales de Tierra in the Gulf of Chiriquí were erroneous due to errors in data entry. We used previously established age models [*Toth et al.*, 2012; *Toth*, 2013] to sample the cores at the highest temporal resolution between ~6750 cal B.P. and present. Particular attention was given to the period surrounding the depositional hiatus ~4100–1600 cal B.P., as no corals could be sampled during this period in the cores from Iguana, Coiba, or Canales de Tierra. We obtained one sample at the onset of the hiatus ~3795 cal B.P. in a core from Contadora and two samples at ~3150 cal B.P. from Uva, when reef development briefly resumed at this site.

Reef frameworks in the TEP are built primarily by the branching coral *Pocillopora damicornis* [*Toth et al.*, 2012; *Toth*, 2013], and 38 of the 42 corals we sampled were *Pocillopora* spp. The remaining four samples were from

the ahermatypic coral *Psammocora stellata*. High turbidity (low light) restricts reef growth to the upper 10 m of the water column in Pacific Panamá, and both taxa are most common in depths <5 m [*Glynn*, 1976]. In contrast, the average thermocline depth in Pacific Panamá during the rainy (nonupwelling) season is ~50 m [*D'Croz and O'Dea*, 2007]. Measurements of radiocarbon variability from shallow-water *Pocillopora* spp. and *P. stellata* should, therefore, provide a high-fidelity proxy of upwelling in the past.

Each 0.5 to 3 mg coral was broken into two samples for dating. One sample was dated by H. C. and R. L. E. with uranium-series methodologies using inductively coupled plasma–mass spectrometry (Table S1 in the supporting information). The other half was radiocarbon dated by accelerator mass spectrometry (AMS) at Beta Analytic, Inc., Miami, FL, or the National Ocean Sciences AMS facility at the Woods Hole Oceanographic Institution, Woods Hole, MA (Table S2). Our previous analysis (by scanning electron microscopy) of the subfossil coral record from the Gulf of Panamá demonstrated that diagenetic alteration was negligible in samples that passed initial taphonomic screening [*Toth et al*., 2015]. Furthermore, coral powders used in U-series analysis were generally handpicked under a microscope by H. C. to select the highest-quality samples, and samples analyzed with AMS were cleaned via acid etching prior to analysis. It is unlikely, therefore, that diagenesis had a significant impact on our results overall; however, dates from two corals from Contadora and one coral from Iguana (shown in red in [Tables S1 and S2]) were excluded from the reconstructions because the measured U-series dates were highly inconsistent with the radiocarbon-based age models for the cores and inclusion of the U-series dates would have resulted in a significant reversal in the age models [*Toth*, 2013]. We thus conclude that these three U-series dates were likely contaminated by detrital material.

The measurements from each coral allowed us to calculate a discrete "snapshot" of the radiocarbon age of surface waters in the region. Based on the average growth rates of the corals, each sample represented a measurement across one to two annual cycles [*Glynn*, 1977]. Whereas high-resolution measurements of radiocarbon variability along the growth axis of a coral can be used to reconstruct changes in local oceanography across intra-annual scales [e.g., *Druffel*, 1981, 1982, 1987; *Ingram*, 1998; *Southon et al*., 2002; *Fontugne et al*., 2004; *Druffel et al*., 2008; *Zaunbrecher et al*., 2010], our measures of whole-colony ΔR are time averaged across at least one annual cycle, a time scale over which significant mixing likely occurs within the gulfs. By collecting time-averaged snapshots of radiocarbon variability from the corals, we minimize the possibility that the results would be skewed by a single extreme event (i.e., intensified upwelling during a La Niña event). Our records cannot be used to detect the impacts of individual upwelling events at particular sites, but rather they represent long-term averages of upwelling intensity.

5.2. Marine Reservoir Calculation

U-series dating is not subject to reservoir effects and provides an independent proxy for the "true age" of marine carbonates [*Bard et al*., 1993]. Using the age estimate derived from the U/Th split of each coral sample as cal B.P., we determined the expected ^{14}C age of that sample based on the terrestrial and marine radiocarbon calibration curves: IntCal13 and Marine13, respectively [*Reimer et al*., 2009]. An estimate of the total reservoir age, R, was calculated for each coral sample according to the following equation, where $^{14}C_{conventional}$ is the conventional radiocarbon age:

$$R = {}^{14}C_{conventional} - {}^{14}C_{expected\ (IntCal13)} \quad (1)$$

Similarly, ΔR was calculated as

$$\Delta R = {}^{14}C_{conventional} - {}^{14}C_{expected\ (Marine13)} \quad (2)$$

The error terms for R and ΔR were calculated by combining the 2σ errors associated with the conventional ^{14}C age (SD_1) and expected ^{14}C age from the appropriate calibration curve (SD_2):

$$SD_{combined} = \left[(SD_1)^2 + (SD_2)^2\right]^{0.5} \quad (3)$$

The combined error was used to calculate 95% confidence intervals (CIs) for our estimates of R and ΔR (95% CI = $SD_{combined} \times 1.96$).

5.3. Statistical Analyses

R and ΔR are positively related and vary in concert; therefore, detailed statistical analysis of both proxies would be redundant. Whereas R is a measure of overall changes in surface water radiocarbon from both local and larger-

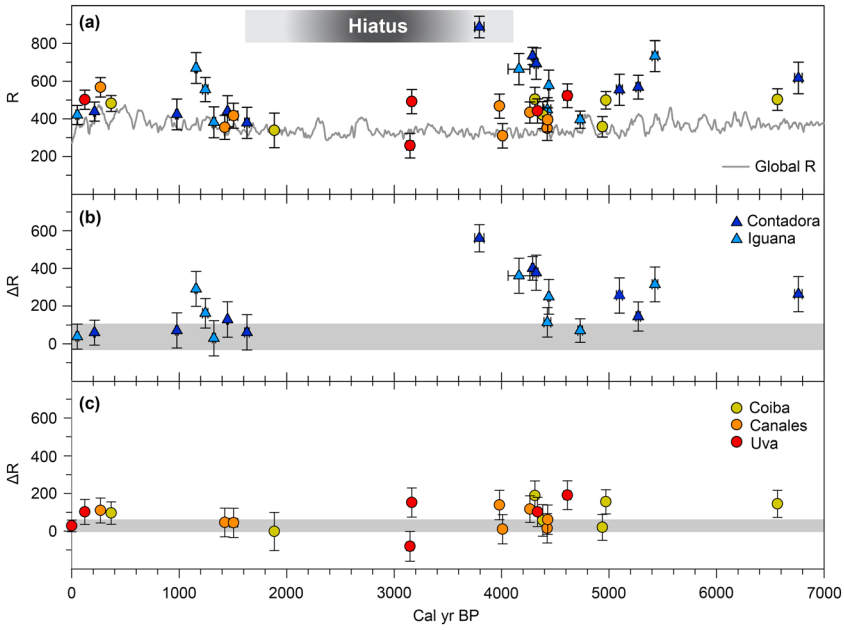

Figure 2. Reconstructions of the total reservoir age, *R*, and the local reservoir correction, Δ*R*, in Pacific Panamá from the middle Holocene to the present are shown in relation to the observed hiatus in reef development. (a) Reconstructed *R* (in years) from five sites in Pacific Panamá plotted in relation to the global reservoir age (gray line). Δ*R* (in years) from (b) the Gulf of Panamá, which experiences seasonal wind-driven upwelling, and (c) the Gulf of Chiriquí where there is putatively no upwelling. The records of Δ*R* are plotted in relation to the 95% confidence interval of the modern Δ*R* value for that gulf (gray shading). All error bars represent 95% confidence intervals.

scale changes in oceanography as well as changes in atmospheric radiocarbon, Δ*R* is specifically a measure of the local deviation from larger-scale trends in marine radiocarbon. Although we report variability in *R* in Figure 2 and in Table 1, we used spatial and temporal variability in Δ*R* as our primary metric for the variability of local upwelling in the past. To determine whether the spatial gradient in upwelling was present through the Holocene, we compared estimates of Δ*R* from the Gulf of Panamá and the Gulf of Chiriquí for 10 time intervals for which the 95% CI of the U/Th ages of samples from the two gulfs overlapped. For each contemporaneous pair, Δ*R* from each gulf was divided by the average values of the pair to standardize the values across multiple time periods. The standardized differences in Δ*R* between gulfs were normally distributed (Shapiro-Wilk test: $W = 0.923$, $P = 0.381$), and the standardized values were compared statistically between gulfs using a paired *t* test.

Temporal variability in Δ*R* was assessed in three ways. First, we compared temporal changes in Δ*R* to the modern Δ*R* for each gulf (Table 1 and Figure 2): 39 ± 67 (95% CI) for the Gulf of Panamá [*Toth et al.*, 2012] (note that we used the adjusted error measurement derived in the present study) and 28 ± 31 for the Gulf of Chiriquí [*Druffel*, 1987]. Δ*R* was considered to vary significantly from the modern value when the 95% CI of modern and Holocene samples did not overlap. Second, we compared Δ*R* between the periods before and after the hiatus in reef development (4100–1600 cal B.P.) using analysis of variance with a general linear model. We chose to analyze each gulf separately because the temporal spread of Δ*R* measurements differed between gulfs and we did not want differences in the temporal ranges of the data to confound the results. For both gulfs, the variances were homogeneous (Levene's test: $W = 1.6096$, $P = 0.222$ and $W = 1.784$, $P = 0.200$), and the residuals were normally distributed (Shapiro-Wilk test: $W = 0.972$, $P = 0.823$ and $W = 0.940$, $P = 0.295$ for the Gulfs of Panamá and Chiriquí, respectively). Finally, we tested the hypothesis that Δ*R* increased in the two gulfs during the runup to the hiatus, 5000–3795 cal B.P., using linear regression analysis. The residuals were normally distributed for both the Gulf of Panamá (Shapiro-Wilk test: $W = 0.917$, $P = 0.451$) and the Gulf of Chiriquí (Shapiro-Wilk test: $W = 0.905$, $P = 0.214$). All statistical analyses were conducted using the software package *R Studio* [*RStudio*, 2013; *R Core Team*, 2014].

6. Results

Calibrated U/Th ages, conventional radiocarbon ages, and the calculated values of *R* and Δ*R* for each sample are presented in Table 1. Our samples ranged in U/Th age from 6761 to 52 cal B.P. Although there was

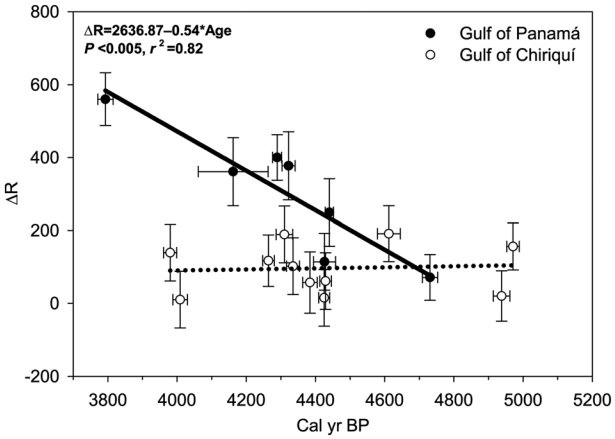

Figure 3. Trends in ΔR (in years) from the Gulf of Panamá (black circles, solid line) and the Gulf of Chiriquí (open circles, dotted line) during the runup to the hiatus in Panamanian reef development. The regression statistics are for the Gulf of Panamá. There were no significant changes in ΔR over time in the Gulf of Chriquí.

considerable spatial and temporal variability, R in Pacific Panamá was generally greater than the global reservoir age (Figure 2a), yielding positive values of ΔR in both gulfs through the Holocene (Figures 2b and 2c). This result highlights the strong impact of upwelling on the shallow-water environments of Pacific Panamá.

6.1. Spatial Variability in ΔR

In the Gulf of Panamá, where upwelling is intense, ΔR averaged 208 years (±34 SE) and varied between 30 and 560 years through the Holocene. In contrast, in the nonupwelling Gulf of Chiriquí, ΔR was both lower on average, 83 years (±16 SE), and less variable, ranging from −81 to 191 years over the same period. Contemporaneous measurements from both gulfs showed that ΔR was significantly higher in the Gulf of Panamá compared with the Gulf of Chiriquí (228% higher on average; $t_9 = 10.167$, $P < 0.001$). Although we did not have enough data to compare ΔR statistically among sites, there appeared to be little spatial variability within gulfs (Figures 2b and 2c).

6.2. Temporal Variability in ΔR

The difference in ΔR between the two gulfs was especially pronounced before the hiatus, whereas ΔR was similar between gulfs during the last 2000 years (Figures 2b and 2c). In the Gulf of Panamá, ΔR was significantly higher and more variable before the hiatus, averaging 282 (±43 SE), compared with only 105 (±31 SE) after ($F_{1,17} = 9.733$, $P = 0.006$); however, there was no difference between these two periods in the Gulf of Chiriquí ($F_{1,16} = 1.290$, $P = 0.273$). During the ~1000 years leading up to the hiatus, ΔR increased dramatically in the Gulf of Panamá (Figure 3; $F_{1,5} = 23.480$, $P < 0.005$, $r^2 = 0.824$), peaking at 560 years at ~3795 cal B.P.; however, ΔR did not change significantly over this period in the Gulf of Chiriquí ($F_{1,9} = 0.044$, $P = 0.839$, $r^2 = -0.106$).

The modern estimates of ΔR in Panamá are low compared with both our estimates from earlier in the Holocene (Figures 2b and 2b) and modern values from elsewhere in the TEP (Figure 1a); however, ΔR was significantly greater than modern during some periods in the past (Table 1 and Figures 2a and 2b). Before the hiatus, there were significant positive deviations in ΔR in both gulfs, but whereas 72% of the ΔR values were significantly higher than modern in the Gulf of Panamá, only 42% were significantly higher than modern in the Gulf of Chiriquí. One measurement of ΔR from Uva Island during the hiatus, from ~3150 cal B.P., was significantly higher than modern, but another from the same time was anomalously low. During the last 2000 years, ΔR was similar to modern in both gulfs with the exception of an anomalously high value from Iguana from ~1150 cal B.P.

7. Discussion

7.1. The Panamanian Upwelling System

Our reconstructions of ΔR suggest that the wind-gap upwelling system has been a significant source of oceanographic variability in Pacific Panamá for at least the last ~6750 years [*Martínez et al.*, 2006; *Toth et al.*, 2012, 2015; *Arellano-Torres et al.*, 2013]. As expected from modern oceanographic records (Figure 1), we detected significant distinctions in the historical oceanography of the two gulfs (Figure 2), confirming our ability to reconstruct mesoscale differences in water-column stratification with ΔR [*Druffel et al.*, 2008; *Zaunbrecher et al.*, 2010]. Whereas upwelling was a dominant process during the Holocene in the Gulf of Panamá, our reconstructions support the conclusion that upwelling was weak to absent in the Gulf of Chiriquí [*Pennington et al.*, 2006; *Alexander et al.*, 2012].

If thermocline shoaling does periodically allow upwelled water to reach shallow-water reef habitats in the Gulf of Chiriquí, as suggested by some researchers [*D'Croz and O'Dea*, 2007], these incursions must have

minor impacts on the regional oceanography relative to the role of upwelling in the Gulf of Panamá. The lack of significant variability in ΔR in the Gulf of Chiriquí during even the most extreme periods of upwelling in the Gulf of Panamá (Figures 2 and 3) indicates that there is little lateral mixing between the gulfs. Similarly, because modern ΔR throughout Pacific Panamá is significantly lower than other nearby locations in the TEP, large-scale advection, which would occur primarily via the Equatorial Undercurrent (Figure 1a) [*Leduc et al*., 2009b], must have a minimal impact on local ΔR, at least at present. Overall, our reconstruction suggests that wind-driven upwelling did not play a significant role in the oceanographic variability of the Gulf of Chiriquí during the Holocene, either directly through water-column mixing or indirectly through lateral mixing with the Gulf of Panamá.

In contrast, lateral mixing was likely common within each of the gulfs during the Holocene [*Pennington et al*., 2006; *D'Croz and O'Dea*, 2007]. Fine-scale oceanographic variability within the two gulfs, which is apparent in modern satellite data sets (Figure 1b), was not observed in our record (Figures 2b and 2c). Within the Gulf of Panamá, for example, SST-based records suggest that modern upwelling is more intense at Contadora compared with Iguana (Figure 1b); however, the range of ΔR was similar at these two sites throughout the Holocene (Figure 2b). The long-term similarity in upwelling between Contadora and Iguana could explain why Holocene reef development followed similar trajectories at the two locations [*Toth et al*., 2012].

Modern estimates of ΔR suggest that the Panamanian upwelling system is less intense than elsewhere in the TEP (Figure 1a); however, our records suggest that contemporary upwelling in the Gulf of Panamá is anomalously weak compared with earlier millennia. Upwelling intensity varied significantly through the Holocene, and the Gulf of Panamá experienced prolonged periods of intense upwelling that exceed any modern estimates from the region (Figure 2b).

7.2. Climatic Drivers of Holocene Upwelling Variability

To identify the primary climatic controls on Panamanian upwelling during the Holocene, we plotted our reconstructions of ΔR alongside proxy records of ENSO variability from the TEP, northern Atlantic temperature, and variability in the mean position of the ITCZ [*Haug et al*., 2001; *Moy et al*., 2002; *Conroy et al*., 2008; *Peterson and Haug*, 2006; *Koutavas and Joanides*, 2012; *Marcott et al*., 2013]. Overall, ENSO variability (Figure 4b) is derived from variance in foraminiferal $\delta^{18}O$ from the cold tongue of the equatorial eastern Pacific (EEP) [*Koutavas and Joanides*, 2012]. We also use *Conroy et al.*'s [2008] record of the percentage of sand in their lake-core record from El Junco, Galápagos (Figure 4c) and *Moy et al.*'s [2002] sediment-color index from Lake Pallcacocha in Equador (Figure 4d) to infer changes in El Niño frequency. Next, we use *Marcott et al.*'s [2013] compilation of sediment-based reconstructions of northern latitude temperature (60–90°N latitude, primarily from the northern Atlantic) as a proxy for broad-scale temperature changes in the northern Atlantic (Figure 4e). Finally, we infer variations in the mean position of the ITCZ from titanium influx to the Cariaco Basin (Figure 4f) [*Haug et al*., 2001; *Peterson and Haug*, 2006].

7.2.1. The Middle Holocene: ~6750–3750 cal B.P.

Our reconstructions demonstrate that the Gulf of Panamá experienced significant fluctuations in upwelling intensity over the last ~6750 years (Figure 4a). Upwelling was significantly stronger and more variable in the first half of our record, ~6750–3795 cal B.P. than later in the Holocene. During the early part of the middle Holocene, ~6750–5000 cal B.P., variability in our record was low and upwelling was moderately intense in the Gulf of Panamá. Existing records of a relatively cool climate [*Koutavas et al*., 2002, 2006; *Koutavas and Joanides*, 2012; *Toth et al*., 2015] and high oceanic productivity [*Loubere et al*., 2003; *Fontugne et al*., 2004; *Warnock et al*., 2007; *Pérez-Cruz*, 2013; *Cabarcos et al*., 2014] in the TEP during this period support our conclusion. Although records from elsewhere in the tropical Pacific show little change in ENSO during the middle Holocene [*Cobb et al*., 2013; *Karamperidou et al*., 2015], most records indicate that ENSO variability and the frequency and intensity of El Niño events were low in the TEP at this time (Figures 4b–4d) [e.g., *Moy et al*., 2002; *Riedinger et al*., 2002; *Rein et al*., 2005; *Rein*, 2007; *Conroy et al*., 2008; *Koutavas and Joanides*, 2012; *Karamperidou et al*., 2015]. Low ENSO variability in the TEP and a strong zonal gradient in sea surface temperatures across the tropical Pacific is consistent with a cool, La Niña-like climate during the middle Holocene [*Koutavas et al*., 2002, 2006; *Koutavas and Joanides*, 2012]. Although a relatively warm climate in the northern Atlantic and a more northerly position of the ITCZ (Figures 4e and 4f) should have suppressed wind-gap upwelling during the middle Holocene, the suppression of strong El Niño events (Figures 4c and 4d) and,

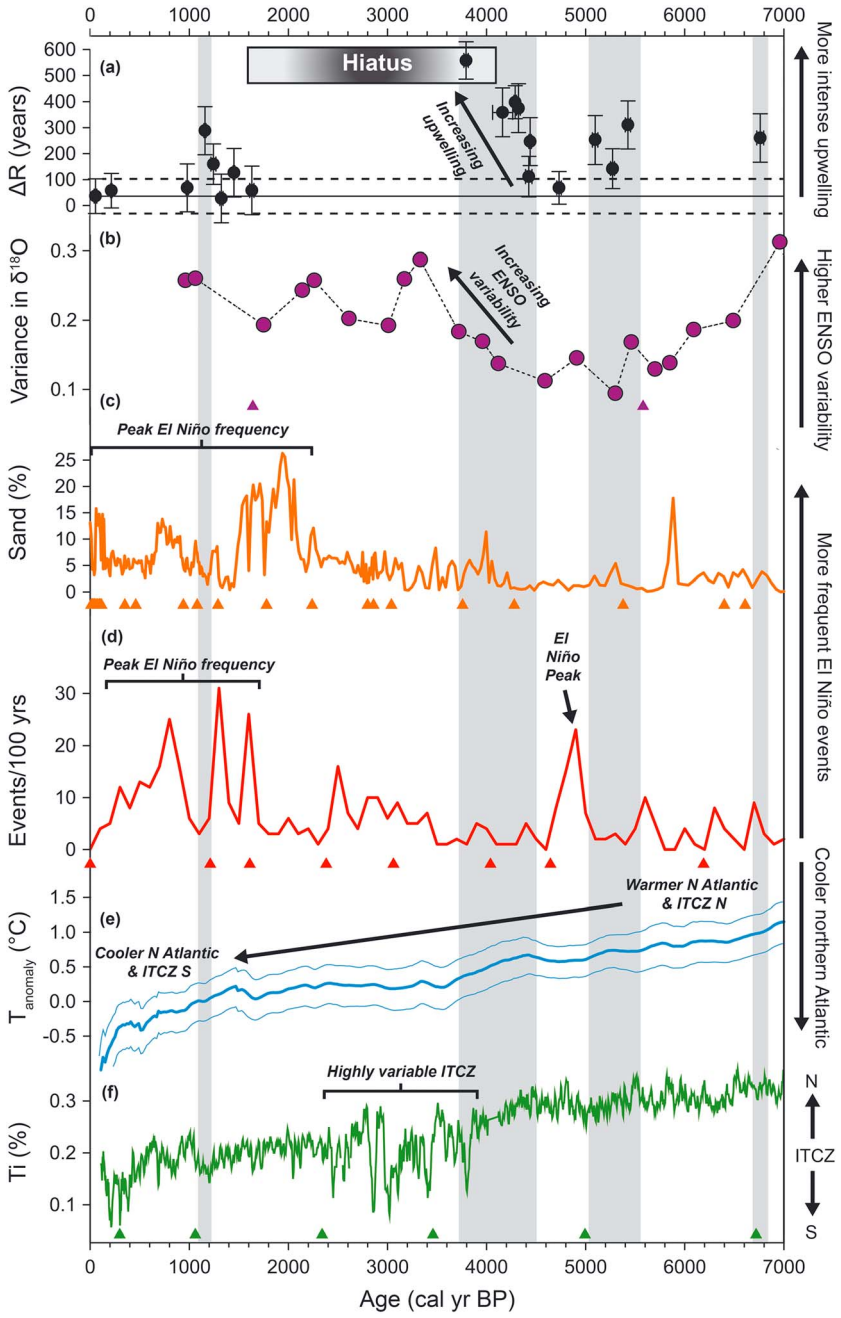

Figure 4. Millennial-scale variability in ΔR compared with proxy records of the potential climatic drivers of wind-gap upwelling: northern Atlantic climate, the ITCZ, and ENSO. (a) ΔR (black points) from the Gulf of Panamá, this study relative to modern value (solid black line). The dashed lines are the 95% CI around the modern value. The points plotting above the dashed line are indicative of significant increases in upwelling intensity. The gray shading running vertically through the panels indicates the intervals when ΔR was significantly higher than modern, indicating stronger-than-modern upwelling. (b) ENSO variability from variance in δ^{18}O in individual foraminifera records from the cold tongue of the equatorial eastern Pacific (purple dots) [*Koutavas and Joanides*, 2012]. (c) El Niño frequency from percent of sand in a core from El Junco Lake, San Cristobal, Galápagos (orange line) [*Conroy et al.*, 2008; *Conroy et al.*, 2008]. (d) El Niño frequency (events per 100 years) from gray scale analysis of a core from Laguna Pallacocha, Ecuador (red line) [*Moy et al.*, 2002]. (e) A multiproxy record of northern latitude (60–90°N) temperature, which reflects millennial-scale changes in northern Atlantic climate (thick blue line). The 1σ uncertainties in the temperature record are plotted as thin blue lines [*Marcott et al.*, 2013]. (f) Variability in the mean latitudinal position of the ITCZ from percent of titanium in a deep-sea core from Cariaco Basin (green line) [*Haug et al.*, 2001]. Key features of the reconstructions are labeled on the figure. Age controls for the climate records are plotted as upward triangles. Because *Marcott et al.*'s [2013] temperature record is a composite reconstruction, it was not possible to indicate the dated intervals for this record. The timing of the hiatus is indicated in Figure 4a.

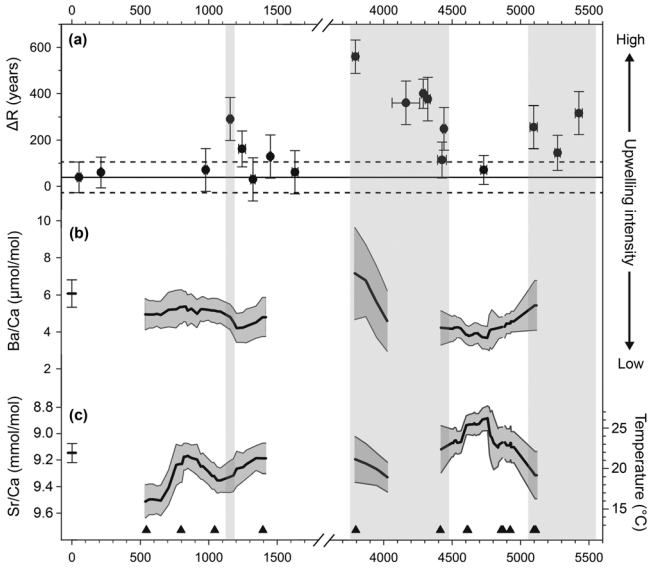

Figure 5. ΔR plotted against coral-based paleoenvironmental reconstructions for Contadora Island, Gulf of Panamá [*Toth et al.*, 2015]. (a) ΔR in the Gulf of Panamá from this study relative to modern value (black line with dashed lines indicating the 95% CI). The gray shading indicates the periods when ΔR was significantly higher than modern, indicating stronger-than-modern upwelling. (b) Ba/Ca-based records of upwelling intensity at Contadora. (c) Sr/Ca-based reconstructions of temperature (see *Toth et al.* [2015] for the Sr/Ca to temperature calibration). Modern Ba/Ca and Sr/Ca are plotted as points (±95% CI). The age controls for *Toth et al.*'s [2015] reconstructions are plotted as upward triangles. Note the break in the figure during the hiatus.

possibly, a cooler mean climate state apparently resulted in overall climatic conditions that favored moderately strong upwelling in Pacific Panamá until ~5000 cal B.P. (Figure 4a).

After 5000 cal B.P., the regime of strong upwelling during the middle Holocene may have been punctuated by a brief decline in upwelling centered at ~4730 cal B.P. (Figure 4a). Our data during this period are limited; however, a centennial-scale weakening in the Panamanian upwelling system is also supported by coral-based Ba/Ca and Sr/Ca records from the Gulf of Panamá, which suggested declines in upwelling and climatic warming from 4700 to 4500 cal B.P. (Figures 5b and 5c) [*Toth et al.*, 2015]. Contemporaneous declines in paleoproductivity of the EEP [*Cabarcos et al.*, 2014] and the Gulf of California [*Pérez-Cruz*, 2013] imply that the drop in productivity may have been a regional phenomenon. The observed decline in regional productivity coincides with a period of relatively low ENSO variability overall [*Koutavas and Joanides*, 2012; *Carré et al.*, 2014], but there is a peak in *Moy et al.*'s [2002] record of El Niño frequency ~4900 cal B.P. (Figure 4). A corresponding peak in El Niño frequency was not observed in *Conroy et al.*'s [2008] record, but *Rein et al.*'s [2005] record from Peru implies that El Niño events were stronger ~5000 cal B.P. Together, these reconstructions suggest that El Niño may have suppressed upwelling in the TEP at this time.

The period of strongest upwelling was in the runup to the hiatus in reef accretion ~4320–3795 cal B.P. Upwelling intensified significantly over this period (Figure 3), and the strongest upwelling in our record ($\Delta R = 560 \pm 72$) was at the beginning of the hiatus at ~3795 cal B.P. (Figures 3 and 4a). Simultaneous increases in the productivity of the EEP [*Cabarcos et al.*, 2014] and coral-based records of climatic cooling (Figure 5c; Sr/Ca) and increased variability and mean of coral-based Ba/Ca (Figure 5b) from Contadora [*Toth et al.*, 2015] reinforce this trend. The coincident decline in titanium influx to the Cariaco Basin (Figure 4f) suggests that a southerly migration of the ITCZ may have contributed to the extreme upwelling at the time; however, it is likely that changing ENSO variability also placed a role. The period of enhanced upwelling coincides with increasing ENSO variability in the TEP (Figure 4b) [*Koutavas and Joanides*, 2012; *Carré et al.*, 2014], a change that likely initiated the onset of high-frequency oscillations in the mean position of the ITCZ (Figure 4f) [*Haug et al.*, 2001]. Although overall variability in ENSO had increased by ~4320–3795 cal B.P. [*Koutavas and Joanides*, 2012; *Carré et al.*, 2014], the frequency and intensity of El Niño events were still relatively low (Figures 4b–4d) [*Moy et al.*, 2002; *Riedinger et al.*, 2002; *Rein et al.*, 2005; *Rein*, 2007; *Conroy et al.*, 2008]. Age uncertainties in the various records could explain the difference in the timing of ENSO versus El Niño intensification; however, another possibility is that the increase in ENSO variability was been driven by enhanced frequency or strength of La Niña, which would explain the increase in Panamanian upwelling. *Toth et al.*'s [2015] paleoenvironmental reconstruction from the Gulf of Panamá (Figures 5b and 5c) and records of a prolonged drought in the Galápagos [*Conroy et al.*, 2008] around this time are consistent with a shift to a La Niña-like state in the TEP; however, there are currently no records of La Niña variability for this period so it is not possible to disentangle the influence of mean climate from that of La Niña per se.

The peak in upwelling coincides with the termination of our record of reef development in the Gulf of Panamá; however, we were able to date two corals from the Gulf of Chiriquí at ~3150 cal B.P. (Table 1 and Figure 2). These records suggest that the hiatus in reef accretion may have been characterized by high oceanographic and climatic variability (Figure 4) [*Haug et al*., 2001; *Koutavas and Joanides*, 2012; *Toth et al*., 2012, 2015]. Indeed, the hiatus was characterized by extremes in the variability of the ITCZ [*Haug et al*., 2001; *Peterson and Haug*, 2006], high ENSO variability [*Koutavas and Joanides*, 2012; *Carré et al*., 2014; *Liu et al*., 2014b], and peaks in the frequency and intensity of El Niño in the TEP (Figure 4) [*Sandweiss et al*., 2001; *Moy et al*., 2002; *Riedinger et al*., 2002; *Rein et al*., 2005; *Rein*, 2007], conditions that likely suppressed reef development in Pacific Panamá for the next ~2000 years [*Toth et al*., 2012, 2015].

7.2.2. The Late Holocene: ~1900 cal B.P. to Present

When reef development resumed during the late Holocene, ~1900 cal B.P. to present, upwelling was, on average, considerably less intense. The only significant excursion in our record of ΔR from the late Holocene occurred ~1150 cal B.P. Our previous environmental reconstructions from Contadora [*Toth et al*., 2015] suggest that there was some climatic cooling at this time (Figure 5c), but there was little response in coral-based Ba/Ca (Figure 5b). Without additional data from this period, we are hesitant to conclude that this single data point reflects a true peak in upwelling, and we therefore focus our discussion of this period on the overall lower ΔR during the last ~1600 years relative to the middle Holocene.

A general decline in oceanic productivity from the middle to late Holocene is supported by a number of existing reconstructions from the TEP (Figure 5) (see *Cabarcos et al*. [2014] for the EEP, *Fontugne et al*. [2004] for the Peruvian upwelling system, and *Toth et al*. [2015] for Pacific Panamá) but is in opposition to the expected increase in the intensity of the northeast trade winds that should result from the southerly migration of the ITCZ and cooling of the northern Atlantic over this period [*Haug et al*., 2001; *Peterson and Haug*, 2006; *Timmermann et al*., 2007; *Xie et al*., 2008; *Sachs et al*., 2009; *Marcott et al*., 2013; *Liu et al*., 2014a; *Schneider et al*., 2014]. Thus, as during the middle Holocene, ENSO or ENSO-like changes in mean climate were likely the strongest controls on Panamá's wind-gap upwelling system in recent millennia.

ENSO variability continued to increase through the late Holocene to present (Figure 4b) [*Koutavas and Joanides*, 2012; *Carré et al*., 2014; *Liu et al*., 2014b], a trend that was likely driven by the high frequency of El Niño events in recent millennia (Figures 4c and 4d) [*Moy et al*., 2002; *Conroy et al*., 2008; but see *Makou et al*., 2010]. Indeed, even though the activity of El Niño was variable during the last ~2000 years, this period was characterized by the highest frequency of El Niño events in the Holocene [*Sandweiss et al*., 2001; *Moy et al*., 2002; *Riedinger et al*., 2002; *Rein et al*., 2005; *Rein*, 2007; *Conroy et al*., 2008]. The period ~1630–980 cal B.P. was a time of particularly high El Niño activity, although the specific timing of El Niño peaks varies among records (Figures 4c and 4d) [*Moy et al*., 2002; *Riedinger et al*., 2002; *Conroy et al*., 2008]. Frequent El Niño event may have acted to suppress wind-gap upwelling at this time [*Philander*, 1990; *Pennington et al*., 2006; *Poveda et al*., 2006].

Because we do not have records of ΔR for the next ~800 years, we cannot discount the possibility that upwelling was stronger at this time. In fact, a record from the Gulf of Papagayo suggested that intense upwelling during the Little Ice Age (LIA) led to the shutdown of reef development in that region [*Glynn et al*., 1983]. Our previous reconstructions from the beginning of the LIA were consistent with climatic cooling (Figure 5c) but not necessarily stronger upwelling (Figure 5d) [*Toth et al*., 2015]. Targeted sampling of this interval is needed therefore to determine the interactions between regional climate during the LIA and wind-gap upwelling.

Upwelling was especially weak during the most recent periods covered by our record: ~210 and 50 cal B.P. The last 200 years were generally characterized by climatic warming in the TEP, but it is not clear whether this trend was driven by enhanced El Niño activity per se [*Conroy et al*., 2009]. Whereas a number of records suggest consistently high El Niño frequency and intensity during this period [*Sandweiss et al*., 2001; *Rein et al*., 2005; *Rein*, 2007; *Conroy et al*., 2008], *Moy et al.*'s [2002] record indicates that El Niño activity was declining at this time (Figures 4c and 4d). Thus, we cannot discount the possibility that a shift in mean climate may have contributed to the weak modern upwelling in the Gulf of Panamá.

Whereas a La Niña-like climate dominated the middle Holocene [*Pennington et al*., 2006; *Conroy et al*., 2008; *Koutavas et al*., 2002, 2006; *Koutavas and Joanides*, 2012], the regime of weakened coastal upwelling during much of the late Holocene is consistent with the hypothesized shift to a more El Niño-like climate

[*Fontugne et al*., 2004; *Pennington et al*., 2006; *Koutavas and Joanides*, 2012; *Pérez-Cruz*, 2013; *Cabarcos et al*., 2014]. Although this shift was primarily driven by the high frequency of El Niño events during the last ~2000 years, mean climate may have also contributed to the decline in upwelling in recent centuries. The combination of a shift in mean climate and an overall increase in ENSO variability driven by more frequent El Niño events (Figures 4b–4d) would have periodically suppressed upwelling [*Philander*, 1990; *Pennington et al*., 2006], decreasing the supply of waters depleted in ^{14}C to the surface over centennial to millennial time scales.

7.2.3. ENSO Drove Long-Term Variability of Upwelling

Previous records have suggested that the ITCZ and by extension northern Atlantic climate [*Timmermann et al*., 2007; *Xie et al*., 2008] played a dominant role in controlling changes in upwelling and oceanic productivity in the TEP during the Holocene [e.g., *Martínez et al*., 2006; *Arellano-Torres et al*., 2013; *Pérez-Cruz*, 2013]. Although the ITCZ is the primary driver of upwelling on intra-annual time scales in Pacific Panamá [*Pennington et al*., 2006; *Poveda et al*., 2006], the mean position of the ITCZ was of little importance in driving millennial-scale changes in upwelling, with the possible exception of the period just before the hiatus. Instead, our records suggest that ENSO variability was the primary control of variability in wind-gap upwelling in Pacific Panamá over the last ~6750 years.

The hypothesized shift from a more La Niña-like climate with few El Niño events during the middle Holocene to a climate dominated by El Niño in the late Holocene [*Sandweiss et al*., 2001; *Moy et al*., 2002; *Riedinger et al*., 2002; *Fontugne et al*., 2004; *Koutavas et al*., 2006; *Pennington et al*., 2006; *Conroy et al*., 2008; *Koutavas and Joanides*, 2012; *Pérez-Cruz*, 2013; *Cabarcos et al*., 2014; *Liu et al*., 2014b] drove a significant decline in Panamanian wind-gap upwelling over this period, culminating in the relatively oligotrophic conditions in the Gulf of Panamá at present (Figures 1a, 2b, and 4a). Contemporaneous declines in the productivity of the EEP and the Peruvian upwelling system and changes in the thermocline structure of the EEP have also been attributed to changes in ENSO [*Fontugne et al*., 2004; *Leduc et al*., 2009b; *Cabarcos et al*., 2014]. In a future that may continue to be characterized by high ENSO variability and more extreme El Niño events [*Cai et al*., 2014, 2015; *Kim et al*., 2014], we expect that a regime of relatively weak upwelling should persist in Pacific Panamá in the coming decades.

7.3. Historical Impacts of Upwelling on Marine Ecosystems

In tropical environments, intense upwelling can result in a shift from an oligotrophic environment that favors reef development to a eutrophic environment that favors planktonic food webs [*Birkeland*, 1988]. In other parts of the world, historic intensification of upwelling as a result of tectonic changes have even resulted in regional-scale coral extinctions [*Sheehan*, 2001; *Edinger and Risk*, 1994]. Similarly, enhanced upwelling in the Indo-Pacific associated with glaciation may have caused lasting changes to the biodiversity and biogeography of that region [*Springer and Williams*, 1990; *Montaggioni*, 2005]. As a corollary, the diminution of Caribbean upwelling after the closure of the Panamanian Isthmus by 2 Myr ago resulted in the mass extinction of eutrophilic mollusks and the proliferation of coral reefs throughout the region [*Allmon et al*., 1996; *Budd et al*., 1996; *Leigh et al*., 2014]. *Glynn et al.* [1983] postulated that, more recently, enhanced upwelling in the Gulf of Papagayo during the Little Ice Age resulted in the shutdown of coral-reef development throughout northern Costa Rica. Overall, it is clear that upwelling is a significant driver of reef development over a variety of spatial and temporal scales [*Hallock and Schlager*, 1986; *Birkeland*, 1988].

Differential upwelling along the Pacific coast of Panamá produces gradients of nutrient availability, which in turn control patterns of regional primary productivity [*Pennington et al*., 2006; *D'Croz and O'Dea*, 2007]. As a result of upwelling, the Gulf of Panamá is presently characterized by elevated nutrients [*Pennington et al*., 2006; *D'Croz and O'Dea*, 2007]; seasonal blooms of phytoplankton, zooplankton, and filamentous algae [*Glynn and Stewart*, 1973; *Glynn*, 1977]; and a relatively high abundance of suspension-feeding taxa compared with the Gulf of Chiriquí [*Birkeland*, 1988; *O'Dea et al*., 2012]. The ecological characteristics of this environment, which are relatively eutrophic compared with the Gulf of Chiriquí, act to suppress modern coral-reef development in the Gulf of Panamá [*Glynn and Stewart*, 1973; *Glynn*, 1977; *Birkeland*, 1988]. Increases in planktonic biomass during upwelling events enhance water-column turbidity, which decreases the light available for photosynthesis in corals [*Glynn and Stewart*, 1973; *Kleypas*, 1997]. High levels of water-column nitrate during upwelling events can also suppress calcification in corals [*Kinsey and Davies*, 1979; *Shantz and Burkepile*, 2014]. Furthermore, nutrient enrichment favors the proliferation and growth of suspension feeders that

Table 2. Suggested Age-Specific ΔR Values for Our Sites in Pacific Panamá

Site Name	^{14}C	1σ	ΔR	1σ[b]
Contadora	600	25.0	60.0	34.0
	1520	40.0	71.0	47.2
	2030–2130[a]	67.5	95.0	48.1
	4380	25.0	560.0	36.8
	4590–4600[a]	57.5	392.9	26.6
	5060–5080[a]	62.1	189.5	76.9
	6570	40.0	263.0	48.0
Iguana	495	25.0	39.0	34.0
	1820–1870[a]	78.0	162.0	122.1
	4430–4580[a]	84.6	166.7	127.5
	5360	40.0	315.0	47.2
Canales	725	25.0	110.0	34.0
	1940–1980[a]	55.7	45.0	27.8
	4020	30.0	10.0	39.7
	4130	30.0	139.0	39.7
	4300–4380[a]	66.7	67.8	59.9
Uva	600	25.0	102.0	34.0
	3220	30.0	-81.0	40.4
	3470	30.0	152.0	39.7
	4320	30.0	102.0	39.7
	4640	30.0	191.0	39.1
Coiba	815	20.0	96.0	30.5
	2280	45.0	−2.0	52.0
	4310–4400[a]	58.5	128.3	93.0
	4730	25.0	20.0	35.4
	4900	20.0	156.0	32.8
	6280	25.0	145.0	36.8

[a]For instances in which the 95% CI of adjacent conventional ^{14}C ages from a site overlapped, we calculated a combined estimate of $\Delta R \pm 1\sigma$ for the overlapping period according to the procedure outlined on the Marine Reservoir Database (http://calib.qub.ac.uk/marine/AverageDeltaR.html).

[b]We report 1σ rather than 95% CI here because the errors in ΔR are always input into calibration models as 1σ.

compete with corals for space and promote the bioerosion of coral skeletons [*Birkeland*, 1977, 1988; *Glynn*, 1997; *O'Dea et al*., 2012].

Modern reefs in the Gulf of Panamá are small and generally restricted to embayments protected from direct exposure to upwelling currents [*Glynn and Stewart*, 1973], but modern reef development nonetheless continues despite the negative influence of upwelling [*Toth*, 2013]. Although the modern upwelling regime in the Gulf of Panamá is apparently not strong enough to preclude reef development in the Gulf of Panamá at present, stronger upwelling during the middle Holocene helped to suppress reef development at that time [*Toth et al*., 2012, 2015]. The increase in upwelling intensity after ~4500 cal B.P. was associated with a progressive decline in reef accretion [*Toth et al*., 2015], which culminated with the ~2500 year shutdown of Panamanian reef development by ~4100 cal B.P. [*Toth et al*., 2012]. The hiatus in reef development was more protracted in the Gulf of Panamá relative to the Gulf of Chiriquí [*Toth et al*., 2012], which explains why reefs in the Gulf of Chiriquí are thicker than in the Gulf of Panamá [*Glynn and Macintyre*, 1977]. Although large-scale climatic perturbations associated with ENSO were the ultimate cause of reef collapse throughout Pacific Panamá, the negative impacts of upwelling may have made reefs in the Gulf of Panamá more susceptible to climatic perturbations [*Toth et al*., 2012, 2015].

If increasing ENSO variability continues to modulate the strength of Panamá's wind-gap upwelling in the coming decades [*Cai et al*., 2014, 2015; *Kim et al*., 2014], then the impact of upwelling on the development of Panamanian reefs in the future could be minor. *Toth et al.* [2012] demonstrated that after the hiatus, when upwelling intensity was low, the millennial-scale growth rates of reefs in the Gulf of Panamá were similar to those in the Gulf of Chiriquí despite the putative difference in coral growth rates between the gulfs [*Glynn*, 1977]. Although strong upwelling has the potential to disrupt reef development in the long term, a warming climate will be the most likely driver of reef degradation in Pacific Panamá in the future [*Toth et al*., 2015]. Coral reefs throughout the TEP have been devastated in recent decades by temperature-induced coral beaching during El Niño events, and these temperature extremes may become both more frequent and more extreme in the future [*Cai et al*., 2014; *Kim et al*., 2014] as could La Niña events [see *Cai et al*., 2015]. If upwelling intensity in the Gulf of Panamá remains moderate in the coming decades, then the negative impacts of upwelling may be outweighed by the potential of cool upwelled waters to buffer against the warmer sea temperatures [*Chollett et al*., 2010; *Smith et al*., 2014]. Whereas extreme upwelling left reefs in Pacific Panamá more vulnerable to climatic extremes in the past, moderate upwelling systems like the modern-day Gulf of Panamá may provide critical refuges that protect reefs against warming sea temperatures in the future [*Riegl and Piller*, 2003; *Karnauskas and Cohen*, 2012; *Smith et al*., 2014].

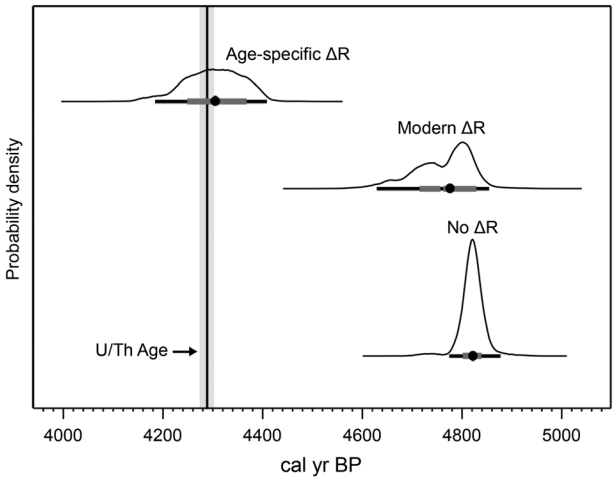

Figure 6. Visual representation of the error associated with using an improper ΔR value for radiocarbon calibrations. We calibrated the conventional ^{14}C age, 4600 ± 20, using only the global marine calibration curve (no ΔR) and the modern ΔR value for the Gulf of Panamá ($\Delta R = 39 \pm 34$) and compared those results with the age-specific ΔR for the Gulf of Panamá that we calculated for conventional ^{14}C ages from 4590 to 4600 years. Probability density functions (thin black lines), cal B.P. (black points), 1σ ranges (thick gray lines), and 2σ ranges (thick black lines) from the three calibrations are shown in relation to the (U/Th) age of the sample. Vertical gray shading around the U/Th age represents its 95% CI.

7.4. Implications for Radiocarbon Dating

For marine samples, an appropriate estimate for ΔR is a critical component of accurate radiocarbon calibrations [*Reimer et al.*, 2009]. Although considerable efforts have been made to constrain the regional variability in ΔR [*Reimer et al.*, 2009], for any given location most researchers rely on a single measurement of ΔR, typically from modern samples [*Reimer and Reimer*, 2001]. Our reconstructions of ΔR from Pacific Panamá demonstrate that such corrections may not be appropriate for calibrations over millennial time scales, particularly in areas strongly affected by regional oceanography.

Consider the extreme example of dating a coral from Contadora Island just before the hiatus, when ΔR was significantly higher than modern (Table 1). The conventional ^{14}C age of this sample was 4600 ± 20. We evaluated the impact of using time-specific estimates of ΔR by comparing the U/Th age of the sample—4289 ± 13—to calibrated radiocarbon dates for the same sample based on (1) the global marine calibration (i.e., $\Delta R = 0$), (2) the modern ΔR for the Gulf of Panamá (39 ± 34), and (3) our estimate of ΔR for samples with conventional ^{14}C ages from 4590 to 4600 years: 392.9 ± 26.6 (Table 2). The resulting probability density functions (pdfs) and calibrated ages are plotted in Figure 6.

Although the inherent error increases when the inclusion of any ΔR, only the age-specific ΔR estimate produced a calibrated age that approximates the true age of the sample. The first two calibrations are significantly different and suggest that the sample is ~500 older than its true age (Figure 6). Furthermore, because of asymmetries in the marine calibration curve during this period, the erroneous use of the modern ΔR to calibrate this sample results in a bimodal probability distribution that actually skews the estimate of the calibrated age toward an improbable value (i.e., toward the valley in the pdf).

Clearly, the assumption of a constant ΔR can represent a significant source of error in the development of marine-based age models and, in turn, the interpretation of paleoenvironmental and paleoecological reconstructions of marine environments. In Table 2, we present a suggested temporal model of ΔR for each site included in our study. Although this model should not be applied to locations outside of Pacific Panamá, the values we derived should give a reasonable approximation of changes in ΔR anywhere within the two gulfs. Age-specific reconstructions of ΔR can be both time consuming and costly to produce, but they are critical for regions that may have experienced significant changes in water-column stratification in the past.

8. Conclusions

The Panamanian wind-gap upwelling system has been active since at least ~6750 cal B.P., but the intensity of upwelling in the Gulf of Panamá has varied considerably as a result of regional- to global-scale climatic forcing. Our reconstruction demonstrates that the assumption of a constant reservoir age must be reconsidered, particularly in upwelling regions like Pacific Panamá. Indeed, the modern Panamanian upwelling regime, which was established by ~1630 cal B.P., is significantly less intense and less variable than during the middle Holocene. The most dramatic increase in upwelling intensity occurred between ~4300 and 3795 cal B.P. coincident with the increase in ENSO variability in the tropical Pacific and the shutdown of reef development throughout Pacific Panamá. Upwelling was not the ultimate cause of reef collapse, but the negative influence of upwelling likely increased the vulnerability of reefs in Pacific Panamá to the impacts of extreme climatic variability.

Although the ITCZ is the primary driver of modern variability Panamanian wind-gap upwelling, and may have contributed to the increase in upwelling leading up to the hiatus, the diminution of upwelling from the middle to the late Holocene suggests that long-term latitudinal migrations of the ITCZ had little impact on longer time scales. Similarly, the modeled impacts of northern Atlantic cooling on wind-gap upwelling are not supported by our reconstruction. Instead, we conclude that ENSO was the primary control on upwelling strength in the Gulf of Panamá through the middle to late Holocene. Whereas a La Niña-like climate characterized by a low frequency of El Niño events allowed for strong upwelling in Pacific Panamá during the middle Holocene, anthropogenic climate change may support the persistence of an El Niño-like climate in the coming decades. As a result, the strength of Panamanian wind-gap upwelling will likely be more moderate in the future.

Acknowledgments

Paula Reimer provided invaluable guidance and advice during the formulation of this project. We also thank Dunia Urrego for her assistance in launching this project. This research was funded by a Graduate Student Research Grant from the Geological Society of America, the Lerner–Gray Marine Research Grant of the American Museum of Natural History, grants from the Smithsonian Institution's Marine Science Network, grant OCE-1535007 from the U.S. National Science Foundation, Natural Science Foundation of China grant 41230524, and the U.S Geological Survey Coastal and Marine Geology Program. Field work was carried out under permits from the Republic of Panamá. Any use of trade, firm, or product names is for descriptive purposes only and does not imply endorsement by the U.S. Government. The complete U/Th and ^{14}C data set is available in the SI. This is contribution 136 from the Institute for Research on Global Climate Change at the Florida Institute of Technology.

References

Alexander, M. A., H. Seo, S. P. Xie, and J. D. Stott (2012), ENSO's impact on the gap wind regions of the eastern tropical Pacific Ocean, *J. Clim.*, *25*, 3549–3565.

Allmon, W. D., G. Rosenberg, R. W. Portell, and K. Schneider (1996), Diversity of Pliocene-recent mollusks in the western Altantic: Extinction, origination, and environmental change, in *Evolution and Environment in Tropical America*, edited by J. B. C. Jackson, A. F. Budd, and A. G. Coates, pp. 271–302, Univ. of Chicago Press, Chicago, Ill.

Arellano-Torres, E., M. L. Machain-Castillo, L. A. Contreras-Rosales, L. B. Cuesta-Castillo, and A. C. Ruiz-Fernández (2013), Foraminiferal faunal evidence for glacial-interglacial variations in the ocean circulation and the upwelling of the Gulf Tehuantepec (Mexico), *Mar. Micropaleontol.*, *100*, 52–66.

Bard, E., M. Arnold, R. G. Fairbanks, and B. Hamelin (1993), ^{230}Th-^{234}U and ^{14}C ages obtained by mass spectrometry on corals, *Radiocarbon*, *35*, 191–199.

Birkeland, C. (1977), The importance of rate of biomass accumulation in early successional stages of benthic communities to the survival of coral recruits, paper presented at the 3rd International Coral Reef Symposium, Int. Coral Reef Soc., Miami, Fla.

Birkeland, C. (1988), Geographic comparisons of coral-reef community processes, paper presented at the 6th International Coral Reef Symposium, Int. Coral Reef Soc., Australia.

Budd, A. F., K. G. Johnson, and T. A. Stemann (1996), Plio-Pleistocene turnover and extinctions in the Caribbean coral-reef fauna, in *Evolution and Environment in Tropical America*, edited by J. B. C. Jackson, A. F. Budd, and A. G. Coates, pp. 168–204, Univ. of Chicago Press, Chicago, Ill.

Cabarcos, E., J.-A. Flores, and F. J. Sierro (2014), High-resolution productivity record and reconstruction of ENSO dynamics during the Holocene in the eastern equatorial Pacific using coccolithophores, *Holocene*, *24*, 176–187.

Cai, W., et al. (2014), Increasing frequency of extreme El Niño events due to greenhouse warming, *Nat. Clim. Change*, *4*, 111–116.

Cai, W., et al. (2015), Increased frequency of extreme La Niña events under greenhouse warming, *Nat. Clim. Change*, *5*, 132–137.

Carré, M., J. P. Sachs, S. Purca, A. J. Schauer, P. Braconnot, R. A. Falcón, M. Julien, and D. Lavallée (2014), Holocene history of ENSO variance and asymmetry in the eastern tropical Pacific, *Science*, *345*, 1045–1048.

Chollett, I., P. J. Mumby, and J. Cortés (2010), Upwelling areas do not guarantee refuge for coral reefs in a warming ocean, *Mar. Ecol. Prog. Ser.*, *416*, 47–56.

Cobb, K. M., N. Westphal, H. R. Sayani, E. Di Lorenzo, H. Cheng, R. L. Edwards, and C. D. Charles (2013), Highly variable El Niño–Southern Oscillation throughout the Holocene, *Science*, *339*, 67–70.

Conroy, J. L., J. T. Overpeck, J. E. Cole, T. M. Shanahan, and M. Steinitz-Kannan (2008), Holocene changes in eastern tropical Pacific climate inferred from a Galápagos lake sediment record, *Quat. Sci. Rev.*, *27*, 1166–1180.

Conroy, J. L., A. Restrepo, J. T. Overpeck, M. Steinitz-Kannan, J. E. Cole, M. B. Bush, and P. A. Colinvaux (2009), Unprecedented recent warming of surface temperatures in the eastern tropical Pacific Ocean, *Nat. Geosci.*, *2*, 46–50.

Corrège, T., T. Delcroix, J. Réey, W. Beck, G. Cabioch, and F. Le Cornec (2000), Evidence for stronger El Niño-Southern Oscillation (ENSO) events in a mid-Holocene massive coral, *Paleoceanography*, *15*, 465–470, doi:10.1029/1999PA000409.

D'Croz, L., and A. O'Dea (2007), Variability in upwelling along the Pacific shelf of Panama and implications for the distribution of nutrients and chlorophyll, *Estuarine Coastal Shelf Sci.*, *73*, 325–340.

Druffel, E. M. (1981), Radiocarbon in annual coral rings from the eastern tropical Pacific Ocean, *Geophys. Res. Lett.*, *8*, 59–62, doi:10.1029/GL008i001p00059.

Druffel, E. M. (1982), Banded corals: Changes in oceanic carbon-14 during the Little Ice Age, *Science*, *218*, 13–19.

Druffel, E. R. M. (1987), Bomb radiocarbon in the Pacific: Annual and seasonal timescale variations, *J. Mar. Res.*, *45*, 667–698.

Druffel, E. R. M., L. F. Robinson, S. Griffin, R. B. Halley, J. R. Southon, and J. F. Adkins (2008), Low reservoir ages for the surface ocean from mid-Holocene Florida corals, *Paleoceanography*, *23*, PA2209, doi:10.1029/2007PA001527.

Edinger, E. N., and M. J. Risk (1994), Oligocene-Miocene extinction and geographic restriction of Caribbean corals: Roles of turbidity, temperature, and nutrients, *Palaios*, *9*, 576–598.

Fontugne, M., M. Carré, I. Bentaleb, M. Julien, and D. Lavallée (2004), Radiocarbon reservoir age variations in the South Peruvian upwelling during the Holocene, *Radiocarbon*, *46*, 531–537.

Glynn, P. W. (1976), Some physical and biological determinants of coral community structure in the eastern Pacific, *Ecol. Monogr.*, *46*, 431–456.

Glynn, P. W. (1977), Coral growth in upwelling and nonupwelling areas off the Pacific coast of Panama, *J. Mar. Res.*, *35*, 567–585.

Glynn, P. W. (1997), Bioerosion and coral-reef growth: A dynamic balance, in *Life and Death of Coral Reefs*, edited by C. Birkeland, Chapman & Hall, New York.

Glynn, P. W., and I. G. Macintyre (1977), Growth rate and age of coral reefs on the Pacific coast of Panamá, presented at the 3th International Coral Reef Symposium, Int. Coral Reef Soc., Miami, Fla.

Glynn, P. W., and R. H. Stewart (1973), Distribution of coral reefs in the Pearl Islands (Gulf of Panamá) in relation to thermal conditions, *Limnol. Oceanogr.*, *18*, 367–379.

Glynn, P. W., E. M. Druffel, and R. B. Dunbar (1983), A dead Central American coral reef tract: Possible link with the Little Ice Age, *J. Mar. Res.*, *41*, 605–637.

Hallock, P., and W. Schlager (1986), Nutrient excess and the demise of coral reefs and carbonate platforms, *Palaios*, *1*, 389–398.

Haug, G. H., K. A. Hughen, D. M. Sigman, L. C. Peterson, and U. Röhl (2001), Southward migration of the Intertropical Convergence Zone through the Holocene, *Science*, *293*, 1304–1308.

Ingram, B. L. (1998), Differences in radiocarbon age between shell and charcoal from a Holocene shellmound in Northern California, *Quat. Res.*, *49*, 102–110.
Karamperidou, C., P. N. Di Nezio, A. Timmermann, F.-F. Jin, and K. M. Cobb (2015), The response of ENSO flavors to mid-Holocene climate: Implications for proxy interpretation, *Paleoceanography*, *30*, 527–547, doi:10.1002/2014PA002742.
Karnauskas, K. B., and A. L. Cohen (2012), Equatorial refuge amid tropical warming, *Nat. Clim. Change*, *2*, 530–534.
Kessler, W. S. (2006), The circulation of the eastern tropical Pacific: A review, *Prog. Oceanogr.*, *69*, 181–217.
Kim, S. T., W. Cai, F.-F. Jin, A. Santoso, L. Wu, E. Guilyardi, and S.-I. An (2014), Response of El Niño sea surface temperature variability to greenhouse warming, *Nat. Clim. Change*, *4*, 786–790.
Kinsey, D. W., and P. J. Davies (1979), Effects of elevated nitrogen and phosphorous on coral reef growth, *Limnol. Oceanogr.*, *24*, 935–940.
Kleypas, J. A. (1997), Modeled estimates of global reef habitat and carbonate production since the Last Glacial Maximum, *Paleoceanography*, *12*, 533–545, doi:10.1029/97PA01134.
Koutavas, A., and S. Joanides (2012), El Niño–Southern Oscillation extrema in the Holocene and Last Glacial Maximum, *Paleoceanography*, *27*, PA4208, doi:10.1029/2012PA002378.
Koutavas, A., J. Lynch-Stieglitz, T. M. Marchitto, and J. P. Sachs (2002), El Niño-like pattern in Ice Age tropical Pacific sea surface temperature, *Science*, *297*, 226–230.
Koutavas, A., P. B. deMenocal, G. C. Olive, and J. Lynch-Stieglitz (2006), Mid-Holocene El Niño-Southern Oscillation (ENSO) attenuation revealed by individual foraminifera in eastern tropical Pacific sediments, *Geology*, *34*, 993–996.
Leduc, G., L. Vidal, K. Tachikawa, and E. Bard (2009a), ITCZ rather than ENSO signature for abrupt climate changes across the tropical Pacific?, *Quat. Res.*, *72*, 123–131.
Leduc, G., L. Vidal, O. Cartapanis, and E. Bard (2009b), Modes of eastern equatorial Pacific thermocline variability: Implications for ENSO dynamics over the last glacial period, *Paleoceanography*, *24*, PA3202, doi:10.1029/2008PA001701.
Leigh, E. G., A. O'Dea, and G. J. Vermeij (2014), Historical biogeography of the Isthmus of Panama, *Biol. Rev.*, *89*, 148–172.
Liu, Z., J. Zhu, Y. Rosenthal, X. Zhang, B. L. Otto-Bliesner, A. Timmermann, R. S. Smith, G. Lohmann, W. Zheng, and O. E. Timm (2014a), The Holocene temperature conundrum, *Proc. Natl. Acad. Sci. U.S.A.*, *111*, E3501–E3505.
Liu, Z., Z. Lu, X. Wen, B. L. Otto-Bliesner, A. Timmermann, and K. M. Cobb (2014b), Evolution and forcing mechanisms of El Niño over the past 21,000 years, *Nature*, *515*, 550–553.
Loubere, P., M. Richaud, Z. Liu, and F. Mekik (2003), Oceanic conditions in the eastern equatorial Pacific during the onset of ENSO in the Holocene, *Quat. Res.*, *60*, 142–148.
Makou, M. C., T. I. Eglinton, D. W. Oppo, and K. A. Hughen (2010), Postglacial changes in El Niño and La Niña behavior, *Geology*, *38*, 43–46.
Manzello, D. P., J. A. Kleypas, D. A. Budd, C. M. Eakin, P. W. Glynn, and C. Langdon (2008), Poorly cemented coral reefs of the eastern tropical Pacific: Possible insights into reef development in a high-CO_2 world, *Proc. Natl. Acad. Sci. U.S.A.*, *105*, 10,450–10,455.
Marcott, S. A., J. D. Shakun, P. U. Clark, and A. C. Mix (2013), A reconstruction of regional and global temperature for the past 11,300 years, *Science*, *339*, 1198–1201.
Martínez, I., D. Rincon, Y. Yokoyama, and T. Barrows (2006), Foraminifera and coccolithophorid assemblage changes in the Panama Basin during the last deglaciation: Response to sea-surface productivity induced by a transient climate change, *Palaeogeogr. Palaeoclimatol. Palaeoecol.*, *234*, 114–126.
Montaggioni, L. F. (2005), History of Indo-Pacific coral reef systems since the last glaciation: Development patterns and controlling factors, *Earth Sci. Rev.*, *71*, 1–75.
Moy, C. M., G. O. Seltzer, D. T. Rodbell, and D. M. Anderson (2002), Variability of El Niño/Southern Oscillation activity at millennial timescales during the Holocene epoch, *Nature*, *420*, 162–165.
O'Dea, A., N. Hoyos, F. Rodríguez, B. De Gracia, and C. Degracia (2012), History of upwelling in the tropical eastern Pacific and the paleogeography of the Isthmus of Panama, *Palaeogeogr. Palaeoclimatol. Palaeoecol.*, *348–349*, 59–66.
Pennington, J. T., K. L. Mahoney, V. S. Kuwahara, D. D. Kolber, R. Calienes, and F. P. Chavez (2006), Primary production in the eastern tropical Pacific: A review, *Prog. Oceanogr.*, *69*, 285–317.
Pérez-Cruz, L. (2013), Hydrological changes and paleoproductivity in the Gulf of California during middle and late Holocene and their relationship with ITCZ and Northern American Monsoon variability, *Quat. Res.*, *79*, 138–151.
Peterson, L. C., and G. H. Haug (2006), Variability in the mean latitude of the Atlantic Intertropical Convergence Zone as recorded by riverine input of sediments to the Cariaco Basin (Venezuela), *Palaeogeogr. Palaeoclimatol. Palaeoecol.*, *234*, 97–113.
Peterson, L. C., G. H. Haug, K. A. Hughen, and U. Röhl (2000), Rapid changes in the hydrologic cycle of the tropical Atlantic during the last glacial, *Science*, *290*, 1947–1951.
Philander, S. G. (1990), *El Niño, La Niña and the Southern Oscillation*, Academic Press, San Diego, Calif.
Poveda, G., P. R. Waylen, and R. S. Pulwarty (2006), Annual and inter-annual variability of the present climate in northern South America and southern Mesoamerica, *Palaeogeogr. Palaeoclimatol. Palaeoecol.*, *234*, 3–27.
R Core Team (2014), *R: A Language and Environment for Statistical Computing*, R Foundation for Statistical Computing, Vienna, Austria. [Available at http://www.R-project.org/.]
Reimer, P. J., and R. W. Reimer (2001), A marine reservoir correction database and on-line interface, *Radiocarbon*, *43*, 461–463.
Reimer, P. J., et al. (2009), IntCal09 and Marine09 radiocarbon age calibration curves: 0–50,000 years cal BP, *Radiocarbon*, *51*, 1111–1150.
Rein, B. (2007), How do the 1982/83 and 1997/98 El Niños rank in a geological record from Peru?, *Quat. Int.*, *161*, 56–66.
Rein, B., A. Lückge, L. Reinhardt, F. Sirocko, A. Wolf, and W.-C. Dullo (2005), El Niño variability off Peru during the last 20,000 years, *Paleoceanography*, *20*, PA4003, doi:10.1029/2004PA001099.
Riedinger, M. A., M. Steinitz-Kannan, W. M. Last, and M. Brenner (2002), A 6100 ^{14}C yr record of El Niño activity from the Galapagos Islands, *J. Paleolimnol.*, *27*, 1–7.
Riegl, B., and W. E. Piller (2003), Possible refugia for reefs in times of environmental stress, *Int. J. Earth Sci.*, *92*, 520–531.
RStudio (2013), RStudio: Integrated development environment for R (version 0.98.978), Boston, Mass. [Available at http://www.rstudio.org/.]
Sachs, J. P., D. Sachse, R. H. Smittenberg, Z. Zhang, D. S. Battisti, and S. Golubic (2009), Southward movement of the Pacific Intertropical Convergence Zone AD 1400–1850, *Nat. Geosci.*, *2*, 519–525.
Sandweiss, D. H., K. A. Maasch, R. L. Burger, J. B. Richardson III, H. B. Rollins, and A. Clement (2001), Variation in Holocene El Niño frequencies: Climate records and cultural consequences in ancient Peru, *Geology*, *29*, 603–606.
Schneider, T., T. Bischoff, and G. H. Haug (2014), Migrations and dynamics of the Intertropical Convergence Zone, *Nature*, *513*, 45–53.
Shantz, A. A., and D. E. Burkepile (2014), Context-dependent effects of nutrient loading on the coral–algal mutualism, *Ecology*, *95*, 1995–2005.
Sheehan, P. M. (2001), History of marine biodiversity, *Geol. J.*, *36*, 231–249.

Smith, T. B., P. W. Glynn, J. L. Maté, L. T. Toth, and J. Gyory (2014), A depth refugium from catastrophic coral bleaching prevents regional extinction, *Ecology*, *95*, 1663–1673.

Soares, A. M. M., and J. M. A. Dias (2006), Coastal upwelling and radiocarbon—evidence for temporal fluctuations in ocean reservoir effect off Portugal during the Holocene, *Radiocarbon*, *48*, 45–60.

Southon, J., M. Kashgarian, M. Fontugne, B. Metivier, and W. W.-S. Yim (2002), Marine reservoir corrections for the Indian Ocean and Southeast Asia, *Radiocarbon*, *44*, 167–180.

Springer, V. G., and J. T. Williams (1990), Widely distributed Pacific plate endemics and lowered sea-level, *Bull. Mar. Sci.*, *47*, 631–640.

Stott, L., C. Poulsen, and R. Thunell (2002), Super ENSO and global climate oscillations at millennial time scales, *Science*, *297*, 222–226.

Timmermann, A., et al. (2007), The influence of a weakening of the Atlantic meridional overturning circulation on ENSO, *J. Clim.*, *20*, 4899–4919.

Toth, L. T. (2013), Holocene coral reef development in the tropical eastern Pacific, Dissertation, Dep. of Biol. Sci., Fla. Inst. of Technol., Melbourne.

Toth, L. T., R. B. Aronson, S. V. Vollmer, J. W. Hobbs, D. H. Urrego, H. Cheng, I. C. Enochs, D. J. Combosch, R. van Woesik, and I. G. Macintyre (2012), ENSO drove 2500-year collapse of eastern Pacific coral reefs, *Science*, *337*, 81–84.

Toth, L. T., R. B. Aronson, K. M. Cobb, H. Cheng, R. L. Edward, P. R. Grothe, and H. R. Sayani (2015), Climatic and biotic thresholds of coral-reef shutdown, *Nat. Clim. Change*, *5*, 369–374.

Warnock, J., R. Scherer, and P. Loubere (2007), A quantitative assessment of diatom dissolution and late Quaternary primary productivity in the eastern equatorial Pacific, *Deep Sea Res., Part II*, *54*, 772–783.

Wyrtki, K. (1965), Surface currents of the eastern tropical Pacific Ocean, *Inter-Am. Trop. Tuna Comm. Bull.*, *9*, 271–304.

Xie, S.-P., Y. Okumura, T. Miyama, and A. Timmermann (2008), Influences of Atlantic climate change on the tropical Pacific via the Central American Isthmus, *J. Clim.*, *21*, 3914–3928.

Zaunbrecher, L. K., K. M. Cobb, J. W. Beck, C. D. Charles, E. R. M. Druffel, R. G. Fairbanks, S. Griffin, and H. R. Sayani (2010), Coral records of central tropical Pacific radiocarbon variability during the last millennium, *Paleoceanography*, *25*, PA4212, doi:10.1029/2009PA001788.

Paleoceanography

Supporting Information for

Holocene variability in the strength of wind-gap upwelling in the tropical eastern Pacific

Lauren T. Toth[1,2], Richard B. Aronson[1], Hai Cheng[3,4], and R. Lawrence Edwards[4]

[1]Department of Biological Sciences, Florida Institute of Technology, 150 West University Boulevard, Melbourne, Florida, 32901
[2] U.S. Geological Survey, Coastal and Marine Science Center, 600 Fourth Street South, Saint Petersburg, Florida, 33701
[3]Institute of Global Environmental Change, Xi'an Jiaotong University, 28 Xianning Road West,
Xi'an, 710049, China
[4]Department of Earth Sciences, University of Minnesota, 310 Pillsbury Dr. SE, Minneapolis, Minnesota, 55455
Corresponding author: Lauren T. Toth, U.S. Geological Survey, 600 Fourth Street South, Saint Petersburg, Florida, 33701. ltoth@usgs.gov

Contents of this file

Site	Sample ID	^{238}U (ppb)	^{232}Th (ppt)	^{230}Th / ^{232}Th (atomic x 10^{-6})	$\delta^{234}U$ (measured)	^{230}Th / ^{238}U (activity)	^{230}Th Age (yr) (uncorrected)	^{230}Th Age (yr) (corrected)	$\delta^{234}U_{Initial}$ (corrected)	^{230}Th Age (yr BP) (corrected)
Contadora	EP08-25-45	2403±3	257±6	444±14	145.6±1.9	0.0029±0.0001	274±6	272±7	146±2	**212±7**
	EP08-25-90	2414±4	580±12	748±18	143.8±2.2	0.0109±0.0001	1045±12	1038±12	144±2	**978±12**
	EP09-27-95	2442±3	754±15	844±17	142.0±1.9	0.0158±0.0001	1518±6	1510±8	143±2	**1450±8**
	EP09-27-130	2453±2	2953±59	245±5	143.3±1.4	0.0179±0.0001	1720±6	1690±22	144±1	**1630±22**
	EP09-28-100	2840±3	2525±51	742±15	144.2±1.6	0.0400±0.0002	3878±16	3856±22	146±2	**3793±22**
	EP09-27-145a	2218±2	975±20	1682±34	143.1±1.5	0.0448±0.0001	4360±11	4349±13	145±1	**4289±13**
	EP09-27-145b	2743±2	2279±46	896±18	144.2±1.5	0.0453±0.0001	4403±12	4382±19	146±2	**4322±19**
	EP09-28-200	2595±3	541±11	4186±88	144.4±1.9	0.0530±0.0002	5161±26	5156±27	146±2	**5096±27**
	EP08-26-305	2720±3	471±10	5213±116	144.5±1.6	0.0547±0.0002	5336±20	5331±20	147±2	**5271±20**
	EP09-28-250	2326±6	585±13	4553±99	142.2±2.3	0.0694±0.0003	6829±35	6823±35	145±2	**6761±35**
	EP08-24-145	2299±2	244±7	1565±51	145.4±1.7	0.0101±0.0002	964±15	961±16	146±2	901±16
	EP08-26-175	2235±3	565±12	4198±92	143.7±1.9	0.0644±0.0003	6315±34	6309±34	146±2	6249±25
Iguana	EP07-16-50	2023±2	200±6	200±24	144.0±1.8	0.0012±0.0001	115±13	112±14	144±2	**52±14**
	EP07-16-100	2329±2	1042±21	472±10	143.2±1.4	0.0128±0.0001	1229±7	1217±11	144±1	**1157±11**
	EP07-17-130	2538±7	1019±22	563.7±15.5	145.2±2.6	0.0137±0.0002	1315±24	1305±25	146±3	**1243±25**
	EP07-15-110	2612±4	1838±37	342±7	144.9±2.4	0.0146±0.0001	1401±10	1383±16	145±2	**1323±16**
	EP07-16-120a	2549±3	14194±284	133±3	145.1±2.0	0.0449±0.0001	4363±16	4222±101	147±2	**4162±101**
	EP07-17-135	2404±6	764±16	2394.4±53.2	141.5±2.1	0.0461±0.0003	4496±31	4488±32	143±2	**4426±32**
	EP07-16-120b	2331±2	637±13	2799±57	145.3±1.3	0.0464±0.0001	4507±11	4500±12	147±1	**4440±12**
	EP07-15-230	2040±3	771±16	2154±44	144.7±1.8	0.0493±0.0002	4801±21	4791±22	147±2	**4731±22**
	EP11-48-315	2399±4	567±13	3917±90	140.9±2.4	0.0561±0.0015	5497±27	5491±27	143±2	**5427±27**
	EP07-16-95	3200±5	854±17	3809±79	142.3±2.2	0.0617±0.0002	6047±25	6040±25	145±2	5980±25
Coiba	EP14-57-50	2583±4	606±13	322±10	144.4±1.9	0.0046±0.0001	437±11	431±11	145±2	**367±11**
	EP13-53-65	2446±4	126±5	6476±265	143.0±2.1	0.0203±0.0001	1950±14	1949±14	144±2	**1885±14**
	EP14-57-95	2312±4	1557±32	1105±23	142.7±2.1	0.0451±0.0002	4391±21	4374±24	144±2	**4310±24**
	EP14-57-120	2842±6	900±18	2389±50	145.3±2.4	0.0459±0.0002	4456±20	4448±21	147±2	**4384±21**
	EP14-57-250	3061±6	2100±42	1239±25	144.7±2.3	0.0515±0.0002	5019±21	5002±24	147±2	**4938±24**
	EP14-57-270	2900±5	379±8	6535±143	146.3±2.0	0.0518±0.0002	5038±18	5035±18	148±2	**4971±18**
	EP13-53-140	2049±3	515±11	4416±93	139.7±1.6	0.0674±0.0002	6637±24	6630±24	142±2	**6566±24**
Canales de Tierra	EP11-43-80	2356±4	328±8	416±19	143.6±2.1	0.0035±0.0001	335±13	332±13	144±2	**268±13**
	EP10-34-180	2048±2	37±3	14152±1157	144.4±1.4	0.0155±0.0001	1487±10	1486±10	145±1	**1424±10**
	EP10-35-205	2077±3	3547±72	162±4	143.5±2.5	0.0168±0.0002	1612±24	1568±39	144±2	**1506±39**
	EP11-42-170	2022±3	178±5	7805±239	145.0±1.7	0.0417±0.0002	4046±19	4044±19	147±2	**3980±19**
	EP11-43-175	2730±5	1035±21	1828±38	142.6±2.4	0.0420±0.0002	4083±19	4073±21	144±2	**4009±21**
	EP11-43-275	2733±5	389±8	5153±112	142.8±2.1	0.0445±0.0002	4332±17	4328±17	145±2	**4264±17**
	EP10-34-210	2328±2	41±4	42799±4363	142.9±1.5	0.0461±0.0001	4487±16	4487±16	145±1	**4425±16**
	EP10-35-230	2475±3	87±5	21598±1141	143.2±1.6	0.0462±0.0002	4492±17	4491±17	145±2	**4429±17**
Uva	EP11-44-130	2249±4	159±5	458±31	142.7±2.5	0.0020±0.0001	188±11	186±11	143±3	**122±11**
	EP10-37-90	2283±6	33±7	38181±7791	140.4±2.3	0.0331±0.0003	3209±31	3209±31	142±2	**3147±31**
	EP10-36-95	2595±5	131±6	10965±542	147.1±1.9	0.0335±0.0002	3226±24	3225±24	148±2	**3163±24**
	EP10-37-140	2130±4	60±4	26671±1608	145.2±2.1	0.0453±0.0002	4400±19	4399±19	147±2	**4335±19**
	EP10-37-205	2522±7	100±6	19827±1175	140.5±2.6	0.0479±0.0003	4675±33	4674±33	142±3	**4612±33**

Table S1. U/Th ages in years before present (yr BP; where present is 1950 C.E.) used as the "true ages" of coral samples when calculating R and ΔR. The Sample ID includes the date the core was collected, the core number, and the depth of the sample in the core. For example, EP08-25-45, indicates that the core was the 25th core collected in the eastern Pacific (EP), that it was collected in 2008, and that the sample collected for dating came from 45 cm depth in the core. $\delta^{234}U_{measured} = ([^{234}U/^{238}U]_{activity} - 1) * 1000$. $\delta^{234}U_{initial}$ was calculated based on ^{230}Th age (T), i.e., $\delta^{234}U_{initial} = \delta^{234}U_{measured} * e^{\lambda 234T}$. All initial d234U values are with error of, or very close to the modern marine value, and show no evidence of open system behavior. Corrected ^{230}Th ages assume the initial $^{230}Th/^{232}Th$ atomic ratio of 4.4 ±2.2x10^{-6}. Those are the values for a material at secular equilibrium, with the bulk-earth $^{232}Th/^{238}U$ value of 3.8. All errors are reported as 2σ. Dates in red, which correspond to the ^{14}C ages in red in Table S2, were excluded because they were inconsistent with the existing ^{14}C-based age models for the cores.

Site	Sample ID	Accession #	F_m measured	$\delta^{13}C$	F_m corrected	Conventional ^{14}C age
Contadora	EP08-25-45	OS-92974	0.9707±0.0029	-2.7	0.9278±0.0029	**600±25**
	EP08-25-90	Beta-283578	0.8666±0.0041	-2.5	0.8276±0.0041	**1520±40**
	EP09-27-95	Beta-279447	0.8122±0.0040	-3.0	0.7766±0.0038	**2030±40**
	EP09-27-130	Beta-279446	0.8032±0.0039	-2.5	0.7670±0.0038	**2130±40**
	EP09-28-100	OS-114153	-	-2.7	0.5798±0.0017	**4380±25**
	EP09-27-145a	OS-112126	-	-3.1	0.5640±0.0013	**4600±20**
	EP09-27-145b	Beta-279445	0.5913±0.0029	-2.5	0.5647±0.0028	**4590±40**
	EP09-28-200	Beta-283575	0.5571±0.0026	-2.1	0.5313±0.0026	**5080±40**
	EP08-26-305	OS-92972	0.5575±0.0021	-2.3	0.5324±0.0021	**5060±40**
	EP09-28-250	OS-92975	0.4618±0.0022	-2.9	0.4415±0.0022	**6570±40**
	EP08-24-145	Beta-283573	0.8042±0.0038	-3.2	0.7690±0.0038	2110±40
	EP08-26-175	Beta-283574	0.6590±0.0031	-1.7	0.6286±0.0031	3730±40
Iguana	EP07-16-50	OS-92973	0.9835±0.0022	-2.7	0.9399±0.0029	**495±25**
	EP07-16-100	Beta-279450	0.8286±0.0041	-3.3	0.7923±0.0039	**1870±40**
	EP07-17-130	Beta-298142	0.8317±0.0030	-3.7	0.7963±0.0030	**1830±30**
	EP07-15-110	Beta-283576	0.8338±0.0040	-2.8	0.7973±0.0040	**1820±40**
	EP07-16-120a	Beta-279449	0.5995±0.0029	-2.4	0.5725±0.0028	**4480±40**
	EP07-17-135	Beta-298143	0.6018±0.0022	-3.9	0.5761±0.0022	**4430±30**
	EP07-16-120b	Beta-279448	0.5920±0.0029	-2.7	0.5654±0.0028	**4580±40**
	EP07-15-230	OS-112127	-	-2.4	0.5654±0.0014	**4580±20**
	EP11-48-315	OS-95738	-	-2.7	0.5131±0.0025	**5360±40**
	EP07-16-95	Beta-283577	0.8317±0.0040	-2.4	0.7943±0.0040	1850±40
Coiba	EP14-57-50	OS-112125	-	-2.1	0.9037±0.0020	**815±20**
	EP13-53-65	OS-112071	-	-1.9	0.7532±0.0041	**2280±45**
	EP14-57-95	OS-112077	-	-2.3	0.5780±0.0022	**4400±30**
	EP14-57-120	OS-112076	-	-1.9	0.5845±0.0027	**4310±35**
	EP14-57-250	OS-112075	-	-2.2	0.5549±0.0016	**4730±25**
	EP14-57-270	OS-112073	-	-1.4	0.5432±0.0015	**4900±20**
	EP13-53-140	OS-112072	-	-3.8	0.4578±0.0013	**6280±25**
Canales	EP11-43-80	OS-92994	0.9571±0.0031	-2.1	0.9137±0.0031	**725±25**
de Tierra	EP10-34-180	Beta-298144	0.8204±0.0029	-3.4	0.7854±0.0029	**1940±30**
	EP10-35-205	Beta-298146	0.8184±0.0029	-2.6	0.7815±0.0029	**1980±30**
	EP11-42-170	OS-97546	-	-2.4	0.5980±0.0024	**4130±30**
	EP11-43-175	OS-92996	0.6334±0.0023	-3.1	0.6059±0.0023	**4020±30**
	EP11-43-275	OS-92997	0.6143±0.0020	-1.5	0.5857±0.0020	**4300±25**
	EP10-34-210	Beta-298145	0.6093±0.0022	-3.5	0.5833±0.0022	**4330±30**
	EP10-35-230	Beta-298147	0.6078±0.0022	-1.7	0.5797±0.0022	**4380±30**
Uva	EP11-44-130	OS-104261	-	-2.2	0.9281±0.0032	**600±25**
	EP10-37-90	Beta-300908	0.7013±0.0025	-2.4	0.6698±0.0025	**3220±30**
	EP10-36-95	OS-92976	0.6791±0.0023	-2.7	0.6490±0.0023	**3470±30**
	EP10-37-140	Beta-300909	0 .610±0.0022	-3.7	0.5840±0.0022	**4320±30**
	EP10-37-205	Beta-300910	0.5884±0.0021	-1.8	0.5612±0.0021	**4640±30**

Table S2. Radiocarbon ages of coral samples measured with accelerator mass spectrometry (AMS) at Beta Analytic, Inc. or the National Ocean Science AMS facility (NOSAMS). Coral samples were oxidized to CO_2 by hydrolysis and then were converted to graphite for AMS counting. The measured fraction of modern radiocarbon (F_m measured) in each sample was corrected for isotopic fractionation of ^{14}C to ^{13}C according to the following equation F_m corrected = F_m measured * $[(1-25/1000)/(1+\delta^{13}C/1000)]^2$. For NOSAMS samples OS-95738 to OS-114153, $^{13}C/^{12}C$ and $^{14}C/^{12}C$ were measured simultaneously in the AMS system so the measured F_m was already corrected for ^{13}C fractionation. The conventional radiocarbon age is calculated as: Conventional ^{14}C age = -8033 * ln(F_m corrected). All errors are

reported as 1σ. Dates in red, which correspond to the U-series ages in red in Table S2, were excluded because they were inconsistent with the existing ^{14}C-based age models for the cores.